JCB | Journal of Circulating Biomarkers

JCB GENERAL INFORMATION

Aims and Scope

Journal of Circulating Biomarkers is an international, peer-reviewed, open access, scientific, online only journal, published once a year. It focuses on all aspects of the rapidly growing field of circulating blood-based biomarkers and diagnostics using circulating protein and lipid markers, circulating tumor cells (CTC), circulating cell-free DNA (cfDNA) and extracellular vesicles. The journal publishes high-impact articles that deal with all fields related to circulating biomarkers and diagnostics, ranging from basic science to translational and clinical applications. Included within the scope are a broad array of specialties including (but not limited to) cancer, immunology, neurology, metabolic diseases, cardiovascular medicine, regenerative medicine, nosology, physiology, pathology, technological applications in diagnostics, therapeutics, vaccine, drug delivery, regenerative medicine, drug development and clinical trials. The journal also hosts reviews, perspectives and news on specific topics. Interdisciplinary studies are especially suitable for this journal.

Abstracting and Indexing

CNKI Scholar
CrossRef
DOAJ
Ebsco Discovery Service
Embase
Google Scholar
J-Gate
OCLC WorldCat
Opac-ACNP (Catalogo Italiano dei Periodici)
Opac-SBN (Catalogo del servizio bibliotecario nazionale)
PubMed Central
Researcher
ROAD (Directory of Open Access Scholarly Resources)
Scilit
Scimago
Scopus
Sherpa Romeo
Transpose

Publication process

Peer review
Papers submitted to JCB are subject to a rigorous peer review process, to ensure that the research published is valuable for its readership. JCB applies a single-blind review process and does not disclose the identity of its reviewers.

Lead times
Submission to final decision: 6-8 weeks
Acceptance to publication: 2 weeks

Publication fees
All manuscripts are submitted under Open Access terms. Article processing fees cover any other costs, that is no fee will be applied for supplementary material or for colour illustrations. Where applicable, article processing fees are subject to VAT.

Open access and copyright

All articles are published and licensed under Creative Commons Attribution-NonCommercial 4.0 International license (CC BY-NC 4.0).

Author information and manuscript submission

For full author guidelines and online submission visit www.aboutscience.eu

Value of clinical laboratory test for early prediction of mortality in patients with COVID-19: the BGM score

Laura Macias-Muñoz[1]*, Robin Wijngaard[1]*, Bernardino González-de la Presa[1], José Luis Bedini[1,3], Manuel Morales-Ruiz[1-3], Wladimiro Jiménez[1-3]

[1]Department of Biochemistry and Molecular Genetics, Biomedical Diagnostic Center, Hospital Clinic, Barcelona - Spain
[2]Institut d'Investigacions Biomèdiques August Pi i Sunyer (IDIBAPS), Centro de Investigación Biomédica en Red de Enfermedades Hepáticas y Digestivas (CIBERehd), Barcelona - Spain
[3]Department of Biomedicine, University of Barcelona, Barcelona - Spain

*The first two authors are co-authors. Both contributed equally to this study.

ABSTRACT

Background: COVID-19 causes high mortality and long hospitalization periods. The aim of this study was to search for new early prognostic strategies accessible to most health care centers.
Methods: Laboratory results, demographic and clinical data from 500 patients with positive SARS-CoV-2 infection were included in our study. The data set was split into training and test set prior to generating different multivariate models considering the occurrence of death as the response variable. A final computational method called the BGM score was obtained by combining the previous models and is available as an interactive web application.
Results: The logistic regression model comprising age, creatinine (CREA), D-dimer (DD), C-reactive protein (CRP), platelet count (PLT), and troponin I (TNI) showed a sensitivity of 47.3%, a specificity of 98.7%, a kappa of 0.56, and a balanced accuracy of 0.73. The CART classification tree yielded TNI, age, DD, and CRP as the most potent early predictors of mortality (sensitivity = 68.4%, specificity = 92.5%, kappa = 0.61, and balanced accuracy = 0.80). The artificial neural network including age, CREA, DD, CRP, PLT, and TNI yielded a sensitivity of 66.7%, a specificity of 92.3%, a kappa of 0.54, and a balanced accuracy of 0.79. Finally, the BGM score surpassed the prediction accuracy performance of the independent multivariate models, yielding a sensitivity of 73.7%, a specificity of 96.5%, a kappa of 0.74, and a balanced accuracy of 0.85.
Conclusions: The BGM score may support clinicians in managing COVID-19 patients and providing focused interventions to those with an increased risk of mortality.

Keywords: BGM score, Clinical biochemistry, COVID-19, Mortality prediction, Risk score, Serum biomarkers

Introduction

The SARS-CoV-2 virus emerged in the last quarter of 2019 in Wuhan, the capital of Hubei province of China. The disease caused by SARS-CoV-2 virus, named COVID-19 by the World Health Organization, has spread rapidly and globally causing a pandemic with unprecedented clinical, humanitarian, and economic repercussions (1,2). In the absence of reliable data on worldwide seroprevalence, the number of confirmed

infections and deaths exceed 17.8 million and 680,000, respectively. The first studies that analyzed the clinical complications associated with this disease were from China. In this area, many of the patients had mild to moderate symptoms (80%), about 14% had a severe disease course (dyspnea, O_2 saturation ≤93%, pulmonary infiltrates), and about 6% presented with critical progression characterized by respiratory failure, septic shock, and/or multiorgan failure (3). The data accumulated so far from more than 10,000 patients in the European Union and in the New York City area show that among the confirmed cases, 30% required admission and 4% required care in intensive care units (ICUs) due to their critical condition (4,5). In turn, it was observed that mortality is particularly high in the subgroup of patients with advanced age and preexisting comorbidities, among which obesity, hypertension, and diabetes are frequently found (6). It is noteworthy that patients without these associated comorbidities can also present with a critical or severe course of the disease. Therefore, the search for early biomarkers to assess the severity of the pathology and its clinical progression is currently necessary to rationalize the use of hospital resources in ICUs and reduce the mortality associated with COVID-19.

Several clinical laboratory markers, such as lymphocyte (LYMPH) count, lactate dehydrogenase (LDH), and D-dimer (DD), are altered in patients with COVID-19 (7). Other studies have shown significant differences in the concentration of cytokines in blood (interleukin [IL]-6, tumor necrosis factor [TNF]-γ, IL-8, IL-2R) among patients who have required ICU admission and patients who do not (8). In turn, infection biomarkers such as C-reactive protein (CRP), procalcitonin (PCT), and ferritin (FER) increased significantly with the severity of the disease (8). However, despite the research efforts made in the field of laboratory tests, reliable algorithms with early prognostic value have not yet been generated to establish the risk of future complications in patients infected with SARS-CoV-2.

The lack of accurate early prognostic algorithms based on central laboratory testing for COVID-19 has spurred researchers to direct their efforts toward the use of omics tools in the search for potential biomarkers. In a first study published by Shen et al (9), the combination of proteomics and metabolomics allowed the identification of a panel of 22 proteins and 7 metabolites with predictive power to differentiate mild vs. severe COVID-19 with 94% accuracy. A second study published in Cell Systems (10) showed that European researchers identified 27 differentially expressed proteomics biomarkers associated with different grades of COVID-19 severity in hospitalized patients. Despite these positive advances, the technical complexity of these omics tools and their high cost limit their applicability in the clinical arena.

In the context of the vast scope of the SARS-CoV-2 crisis and until we achieve sufficient immunization coverage of the population, we believe that the search for new early prognostic strategies must prioritize their applicability and accessibility to most health care centers. In this line, the objective of our study was to generate predictive algorithms for early stratification of patients with COVID-19 who may be at the risk of developing severe complications. To this aim, we designed a retrospective cross-sectional single-center study in which we evaluated different predictive algorithms for mortality considering demographic factors, clinical factors, and standard laboratory tests usually present in most central clinical laboratories.

Materials and methods

Patient population

Five hundred patients with COVID-19 confirmed by real-time reverse transcription polymerase chain reaction (RT-PCR) in nasopharyngeal exudates were included in this retrospective study. These patients required hospitalization in an ICU, internal medicine, or pneumology ward in our hospital between March and June 2020. The clinical and laboratory data that we collected in our database were the first information available within 48 hours after admission of the patient. Demographic and clinical data were obtained from our hospital information system (SAP Patient Management). The variables included were: age, sex, smoking and drinking habits, asthma, chronic obstructive pulmonary disease (COPD), diabetes mellitus, dyslipidemia, obesity,

hypertension, heart failure, ischemic heart disease, hospitalization days, ICU stay, and in-hospital death. This study was approved by the Ethical Committee of the Hospital Clinic of Barcelona and was conducted following the ethical principles of the 1975 Declaration of Helsinki. The data set is available at the online repository *figshare* with DOI:10.6084/m9.figshare.13252277.

Laboratory measurements

Blood samples were collected in lithium heparin-, ethylenediaminetetraacetic acid-, and citrate-coated blood collection tubes for biochemical, hematological, and coagulation testing, respectively. After centrifugation at 3,000 rpm for 15 minutes, plasma samples were immediately processed. Alkaline phosphatase (ALP), alanine aminotransferase (ALT), aspartate aminotransferase (AST), total bilirubin (TBIL), creatinine (CREA), FER, gamma-glutamyl transferase (GGT), glucose (GLU), LDH, CRP, PCT, and troponin I (TNI) were measured using an Atellica Solution automated analyzer (Siemens Healthineers, Tarrytown, NY, USA). The intra-assay and inter-assay coefficient of variation was lower than 6% and 8%, respectively, in all cases. Hematological parameters (including hemoglobin [HB] and counts of white blood cells [WBC], neutrophils [NEU], LYMPH and platelets [PLT]) were analyzed without centrifugation using an Advia 2120 (Siemens Healthineers, Tarrytown, NY, USA). Finally, the Sysmex 5100 (Sysmex, Kobe, Japan) was used for DD, prothrombin time (PT), and partial thromboplastin time (PTT) analysis.

All the parameters were measured in the Core Laboratory of the Hospital Clinic of Barcelona according to the manufacturer's instructions.

Statistical analysis

Categorical variables were expressed as numbers and percentages and compared using the Chi-square test. Continuous variables were expressed as median and interquartile range (IQR) and were compared by the Mann-Whitney-Wilcoxon test.

The strength of the relationship between the laboratory parameters was assessed using the Pearson or Spearman correlation coefficients. The multivariate statistical analyses conducted were logistic regression (LR) (11), classification tree (CT) through the CART algorithm (12), and artificial neural network (NNet) (13). Missing data were imputed via bagged tree models (11), and the data set was then split into a training and test set. The optimal parameter for each model was determined in the training set, calculating the best averaged predictive performance after 10-fold cross-validation. Additionally, to the previous multivariate models, we generated a computational method, called the BGM score, which provides the survival probability of a patient with COVID-19 considering the variables age, CREA, DD, CRP, PLT, and TNI. We modulated the survival probability of the BGM score as a probabilistic event depending on the survival probability given by the LR ($P_{s(LR)}$), the CT ($P_{s(CT)}$), and the NNet ($P_{s(NNet)}$) models generated from our data set. Further, the $P_{s(LR)}$, $P_{s(CT)}$,

and $P_{s(NNet)}$ were multiplied by their corresponding model accuracies ($Ac_{(LR)}$, $Ac_{(CT)}$, and $Ac_{(NNet)}$; respectively), giving the following equation for the BGM score survival probability: $P_{s(BGM)} = (Ac_{(LR)} \times P_{s(LR)}) \cap (Ac_{(CT)} \times P_{s(CT)}) \cap (Ac_{(NNet)} \times P_{s(NNet)})$. Additionally, the following constraints were applied to the $P_{s(BGM)}$ to incorporate the best predictive features of the LR, CT, and NNet models:

$$P_{S(BGM)} \begin{cases} Ac_{(LR)} \times P_{S(LR)} < 0.5 & Ac_{(LR)} \times P_{S(LR)} \geq 0.5 \\ = 0 \quad Ac_{(CT)} \times P_{S(CT)} < 0.5 & ; = 1 \quad Ac_{(CT)} \times P_{S(CT)} \geq 0.5 \\ Ac_{(NNet)} \times P_{S(NNet)} < 0.5 & Ac_{(NNet)} \times P_{S(NNet)} \geq 0.5 \end{cases}$$

$$P_{S(BGM)} \begin{cases} & Ac_{(LR)} \times P_{S(LR)} < 0.5 \\ = Ac_{(CT)} \times P_{S(CT)} & Ac_{(CT)} \times P_{S(CT)} \geq 0.5 \quad ; \\ & Ac_{(NNet)} \times P_{S(NNet)} < 0.5 \end{cases}$$

$$= Ac_{(NNet)} \times P_{S(NNet)} \begin{cases} Ac_{(LR)} \times P_{S(LR)} < 0.5 \\ Ac_{(CT)} \times P_{S(CT)} < 0.5 \\ Ac_{(NNet)} \times P_{S(NNet)} \geq 0.5 \end{cases}$$

Sensitivity, specificity, positive predictive value, negative predictive value, kappa, total accuracy, and balanced accuracy ([sensitivity+specificity]/2) were calculated for each model considering only the test set (99 cases). All the statistical analyses were performed using public libraries from the Comprehensive R Archive Network (CRAN; http://CRAN.R-project.org) rooted in the open-source statistical computing environment R, version 3.6 (http://www.R-project.org/). A p-value <0.05 was considered statistically significant.

We wrote an interactive web application using the R Shiny package (14) that implements the four multivariate models that we generated in our study. This web application can be used to calculate the survival probability for a patient with COVID-19 and is freely available at the link "https://bgm-hoc.shinyapps.io/Shiny_covid_clinic/."

Results

Five hundred subjects with a confirmed diagnosis for COVID-19 formed the study population. Overall, the median age of the patients was 64 years, 42.6% were female, and patients were discharged within a median of 10 days. The most common comorbid conditions were hypertension (44.2%), dyslipidemia (31.2%), and diabetes mellitus (18.8%). Among the patients recruited, 23.4% required ICU, and 19.4% died during follow-up. The demographic, clinical, and laboratory results of the patients corresponding to the first 48 hours after admission are summarized in Tables I and II.

We evaluated a panel of 12 biochemical, 5 hematological, and 3 coagulation biomarkers for each patient. As shown in Figure 1, we detected the presence of high significant correlations in AST-ALT (r = 0.9, p < 0.001) and WBC-NEU (r = 0.8, p < 0.001). To avoid the presence of multicollinearity bias in multivariate analysis, we excluded the variables AST and NEU for future calculations. We included the rest of the biochemical, demographic, and clinical variables in the multivariate LR model that we designed considering the occurrence of death as a response variable and that we generated performing 10-fold cross-validation. Among all the explanatory

TABLE I - Demographic and clinical characteristics of the patients at the first 48 hours after admission

	Total n = 500	Nonsurvivors n = 97 (19.4%)	Survivors n = 403 (80.6%)	p-value
Female, n (%)	213 (42.6%)	42 (43.3%)	171 (42.4%)	0.96752
Age, median (IQR)	64 (54-76)	80 (72-86)	61 (50-72)	6.50e-25
Active smoker, n (%)	25 (5.0%)	6 (6.2%)	19 (4.7%)	0.73589
Active alcohol consumer, n (%)	15 (3.0%)	4 (4.1%)	11 (2.7%)	0.69568
Asthma, n (%)	25 (5.0%)	5 (5.2%)	20 (5.0%)	1.00000
COPD, n (%)	26 (5.2%)	8 (8.2%)	18 (4.5%)	0.21092
Diabetes, n (%)	94 (18.8%)	30 (30.9%)	64 (15.9%)	0.00111
Dyslipidemia, n (%)	156 (31.2%)	41 (42.3%)	115 (28.5%)	0.01247
Obesity, n (%)	33 (6.6%)	4 (4.1%)	29 (7.2%)	0.38628
Hypertension, n (%)	221 (44.2%)	64 (66.0%)	157 (39.0%)	2.63e-06
Atrial fibrillation, n (%)	37 (7.4%)	10 (10.3%)	27 (6.7%)	0.31576
Heart failure, n (%)	23 (4.6%)	11 (11.3%)	12 (3.0%)	0.00112
Ischemic heart disease, n (%)	31 (6.2%)	14 (14.4%)	17 (4.2%)	0.00045
ICU admission, n (%)	117 (23.4%)	30 (30.9%)	87 (21.6%)	0.06921
Hospitalization days, median (IQR)	10 (6-18)	6 (3-11)	12 (7-20)	9.86e-09

COPD = chronic obstructive pulmonary disease; ICU = intensive care unit; IQR = interquartile range.

TABLE II - Biochemical, hematological, and coagulation parameters determined within the first 48 hours after admission

	Total (n = 500)		Nonsurvivors (n = 97)		Survivors (n = 403)		p-value	Normal range
	n	Median (IQR)	n	Median (IQR)	n	Median (IQR)		
ALP, U/L	491 (98.2%)	68 (55-90)	94 (96.9%)	76 (58-108)	397 (98.5%)	68 (45-86)	0.00342	46-116
ALT, U/L	492 (98.4%)	29 (19-50)	95 (97.9%)	25 (18-48)	397 (98.5%)	29 (19-51)	0.30541	5-40
AST, U/L	487 (97.4%)	38 (27-60)	93 (95.9%)	49 (31-73)	394 (97.8%)	37 (26-56)	0.00974	5-40
TBIL, mg/dL	490 (98.0%)	0.5 (0.4-0.7)	93 (95.9%)	0.6 (0.4-0.9)	397 (98.5%)	0.5 (0.4-0.7)	0.01930	0.2-1.2
CREA, mg/dL	500 (100%)	0.89 (0.71-1.1)	97 (100%)	1.11 (0.87-1.83)	403 (100%)	0.86 (0.69-1.04)	4.60e-10	0.3-1.3
FER, ng/mL	383 (76.6%)	602 (266-1278)	71 (73.2%)	914 (376-1533)	312 (77.4%)	559 (240-1190)	0.00221	15-200
GGT, U/L	491 (98.2%)	39 (25-78)	94 (96.9%)	39 (27-92)	397 (98.5%)	40 (24-76)	0.43835	5-40
GLU, mg/dL	500 (100%)	107 (96-130)	97 (100%)	125 (104-160)	403 (100%)	105 (95-123)	9.95e-07	65-110
LDH, U/L	477 (95.4%)	316 (244-418)	87 (89.7%)	432 (276-583)	390 (96.8%)	301 (240-395)	6.99e-07	<234
CRP, mg/dL	499 (99.8%)	7.3 (3.4-15.1)	97 (100%)	14.3 (7.9-22.8)	402 (99.8%)	6.3 (2.8-11.9)	1.51e-12	<1
PCT, ng/mL	416 (83.2%)	0.11 (0.05-0.25)	77 (79.4%)	0.37 (0.17-1.05)	339 (84.1%)	0.09 (0.04-0.18)	2.40e-19	<0.5
TNI, ng/L	410 (82.0%)	8.5 (3.9-22.8)	77 (79.4%)	45.0 (20.1-112.1)	333 (82.6%)	6.8 (3.2-14.9)	1.05e-21	<45.2
HB, g/L	500 (100%)	137 (126-147)	97 (100%)	130 (114-143)	403 (100%)	139 (128-148)	0.00015	120-170
PLT, ×10⁹/L	500 (100%)	180 (137-227)	97 (100%)	166 (112-220)	403 (100%)	182 (146-231)	0.00130	130-400
WBC, ×10⁹/L	500 (100%)	6.0 (4.5-7.7)	97 (100%)	7.2 (5.4-9.8)	403 (100%)	5.8 (4.4-7.3)	1.89e-05	4-11
LYMPH, ×10⁹/L	500 (100%)	0.8 (0.6-1.1)	97 (100%)	0.6 (0.4-0.9)	403 (100%)	0.9 (0.6-1.2)	5.10e-11	0.9-4.5
NEU, ×10⁹/L	500 (100%)	4.6 (3.2-6.3)	97 (100%)	5.7 (4.5-8.3)	403 (100%)	4.2 (3.1-5.7)	5.17e-08	2-7
DD, ng/mL	450 (90.0%)	700 (400-1300)	79 (81.4%)	1500 (800-4350)	371 (92.1%)	600 (400-1000)	1.96e-11	<500
PT, sec	273 (54.6%)	12.8 (12.1-13.6)	57 (58.8%)	13.1 (12.3-14.3)	216 (53.6%)	12.8 (12.1-13.5)	0.02284	9.9-13.7
PTT, sec	225 (45.0%)	29.7 (27.4-31.8)	55 (56.7%)	29.1 (26.7-31.3)	170 (42.2%)	30.0 (27.9-32.0)	0.11795	23.5-32.5

ALP = alkaline phosphatase; ALT = alanine aminotransferase; AST = aspartate aminotransferase; CREA = creatinine; CRP = C-reactive protein; DD = D-dimer; FER = ferritin; GLU = glucose; GGT = gamma-glutamyl transferase; HB = hemoglobin; LDH = lactate dehydrogenase; LYMPH = lymphocyte count; NEU = neutrophil count; PCT = procalcitonin; PLT = platelet count; PT = prothrombin time; PTT = partial thromboplastin time; TBIL = total bilirubin; TNI = troponin I; WBC = white blood cell count.

variables included initially in the model (variables shown in Tabs. I and II) only age, CREA, DD, CRP, PLT, and TNI were early independent predictors of mortality after admission (Tab. III), according to the model selection rule based on the Akaike information criterion (AIC). This multivariate model yielded a sensitivity of 47.3%, a specificity of 98.7%, a kappa of 0.56, and a balanced accuracy of 0.73 for identifying patients with a high risk of mortality. We obtained these performance characteristics using a validation set of 99 cases that were not used for training the model. Despite the high negative predictive value of the LR model (0.9), we observed a low sensitivity that suggests that the model was sensitive to class imbalance.

To improve our classification performance without down-sampling, we next generated two additional multivariate models based on a different paradigm of categorization, CTs with the CART algorithm (the implementation in R is called rpart) and NNets. Considering all the variables from Tables I and II, the CART CT yielded TNI (cutoff value of 44 ng/L), age (cutoff value of 79 years), DD (cutoff value of 700 ng/mL), and CRP (cutoff value of 15 mg/dL) as the most potent early predictors for stratifying patients with a high vs. low risk of mortality (Fig. 2). These cutoff values were similar to their reference intervals implemented for clinical diagnosis (TNI < 45.2 ng/L, DD < 500 ng/mL, and CRP < 1 mg/dL). This model outperformed the LR model with a sensitivity of 68.4%, a specificity of 92.5%, a kappa of 0.61, and a balanced accuracy of 0.80 for identifying patients with a high risk of mortality in our validation set. Despite this performance comparison, one common characteristic in these models was that both yielded clinical laboratory measurements as the most powerful predictors of mortality in patients with COVID-19.

In general, the outputs of LR and CT are intuitive and easy to implement as predictive algorithms in the clinical setting. However, NNets are black boxes regarding the contribution of the explanatory variables to the output of the response
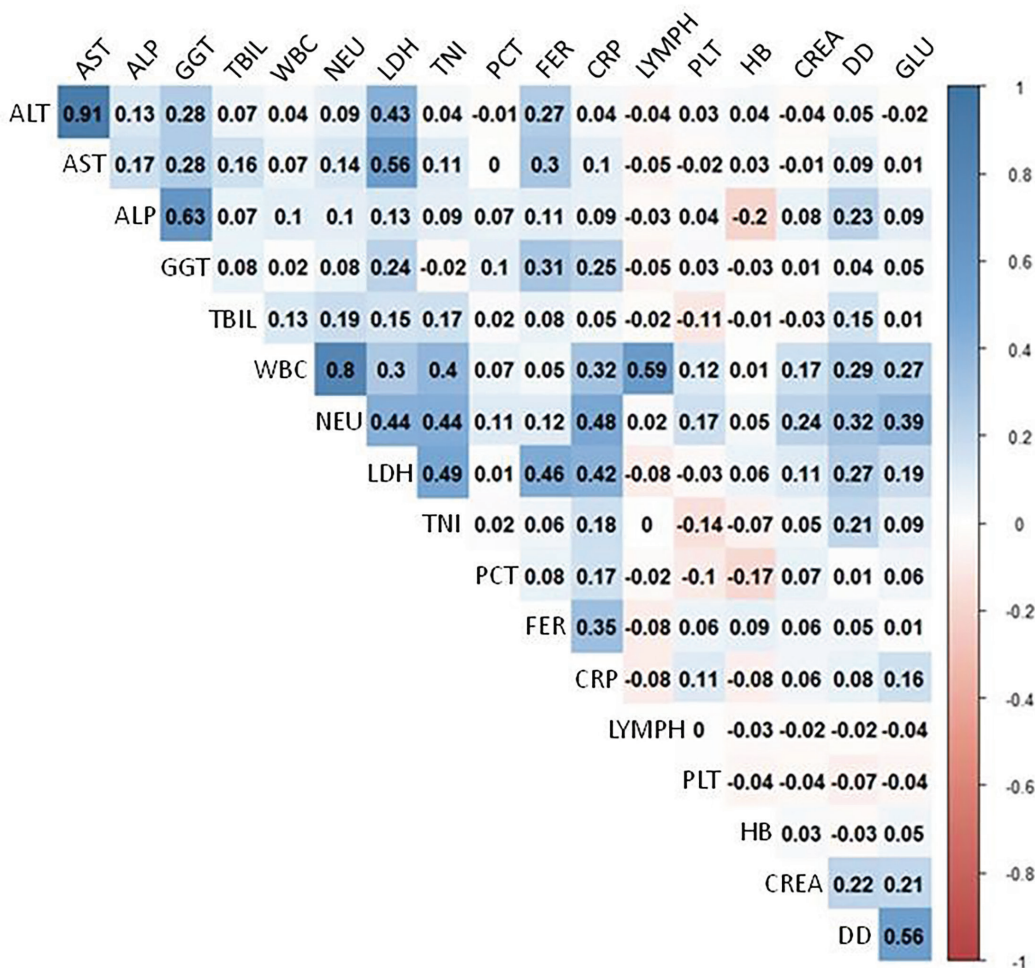
Fig. 1 - Correlation plot. The plot shows the correlation between all the clinical laboratory results obtained within the first 48 hours after patient admission. The bar on the right depicts the equivalence between the color code, and the value of the correlation coefficients shown for each pair of laboratory parameters.
ALP = alkaline phosphatase; ALT = alanine aminotransferase; AST = aspartate aminotransferase; CREA = creatinine; CRP = C-reactive protein; DD = D-dimer; FER = ferritin; GLU = glucose; GGT = gamma-glutamyl transferase; HB = hemoglobin; LDH = lactate dehydrogenase; LYMPH = lymphocyte count; NEU = neutrophil count; PCT = procalcitonin; PLT = platelet count; TBIL = total bilirubin; TNI = troponin I; WBC = white blood cell count.

TABLE III - Logistic regression coefficients for predicting the response variable "survival vs. death" for patients with COVID-19

	Odd ratio	Std. error	Z-statistic	p-value
Age	2.012	1.281	5.665	1.47e-08
CREA	2.573	1.012	2.465	0.01370
DD	2.086	1.000	2.493	0.01266
CRP	2.012	1.828	4.942	7.71e-07
PLT	0.697	1.079	−3.025	0.00249
TNI	1.210	1.000	2.051	0.04031

CREA = creatinine; CRP = C-reactive protein; DD = D-dimer; PLT = platelet count; TNI = troponin I.

variable. Therefore, we have to limit the selection of variables to generate manageable NNet models applicable to most clinical settings regardless of their limitations in their laboratory tests portfolio. In this context, and with the intention intending of improving our LR model, we generated an artificial NNet including only the variables that remained as early independent predictors of mortality in the LR model: age, CREA, DD, CRP, PLT, and TNI. Supplemental figure 1

shows the optimal architecture of the neural model that was obtained after 10-fold cross-validation. The NNet model yielded a sensitivity of 66.7%, a specificity of 92.3%, a kappa of 0.54, and a balanced accuracy of 0.79 for identifying patients with a high risk of mortality in our validation set. This performance was comparable to that achieved by our previous CT algorithm.

The three algorithms we generated can be divided into two groups considering their sensitivity and specificity. The model with the highest specificity was LR, while the CT and NNet models presented lower specificity but a higher sensitivity. These differences in predictive accuracy led to our developing a new hybrid model in combination with the LR, CT, and NNet models to incorporate the best predictive features of each. As described in the Material and Methods, our model, called the BGM score, calculates a survival probability for patients with COVID-19 by multiplying the survival probabilities of the three previous models corrected by their accuracies. We assessed the BGM score performance in terms of prediction accuracy over the validation set, yielding a sensitivity of 73.7%, a specificity of 96.5%, a kappa of 0.74, and a balanced accuracy of 0.85 for the prediction of COVID-19 patients who died. Figure 3 shows the statistical comparison of the accuracies of the four models, where it can be
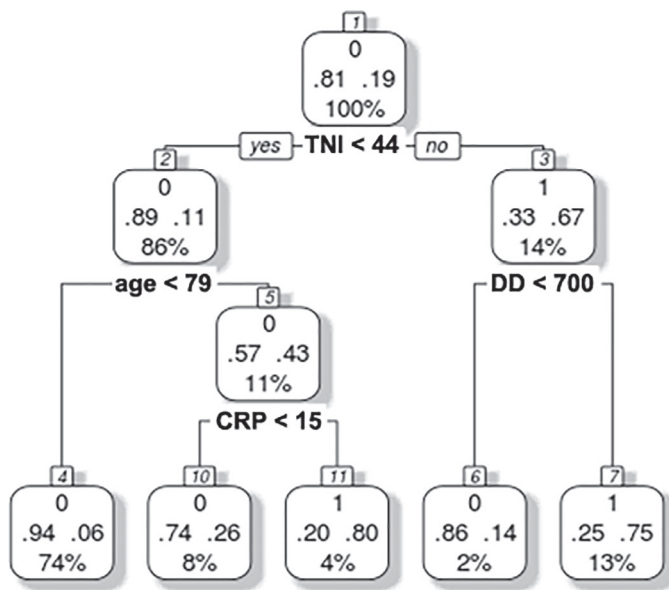
Fig. 2 - Multivariate classification tree analysis. Troponin I (TNI), age, D-dimer (DD), and C-reactive protein (CRP) were the most powerful predictors. The number 0 represents survival and 1 represents death. For each square (leaves), survival and death probabilities are represented with decimal numbers at the left and the right side, respectively, and the percentage represents the number of cases that is split between the leaves of tree partitions.
Units: TNI, ng/mL; age, years; DD, ng/mL; CRP, mg/dL.
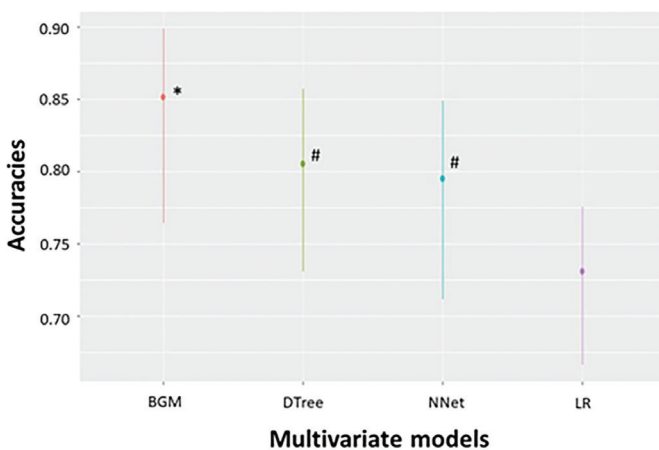
Fig. 3 - Comparison of the accuracy values of the different multivariate models. Logistic regression (LR), decision tree (DTree), neural network (NNet), and the BGM models. The plot shows the accuracy value for each model (horizontal line) and their corresponding 95% confidence interval (vertical lines). *$p < 0.05$ vs. all the models, and #$p < 0.05$ vs. the logistic regression model.

seen that the BGM score model significantly outperformed all the other models. Our hybrid model corroborates the prognostic value of the clinical laboratory tests for patients with COVID-19.

A web application with the implementation of the BGM score model is available at "https://bgm-hoc.shinyapps.io/Shiny_covid_clinic/".

Discussion

This retrospective study identified risk factors for death in hospitalized patients with COVID-19. Older age, lower LYMPH and PLT in addition to higher CREA, DD, CRP, and TNI were independent risk factors for death among patients. Taking this into account, we developed a predictive algorithm for mortality (BGM score) considering standard laboratory tests usually present in most central clinical laboratories.

Concerning biochemical, hematological, and coagulation parameters, our findings are in consonance with those previously described. For instance, a recent published work by Sisó-Almirall et al (15) revealed that LDH, DD, and CRP were the most important laboratory parameters significantly associated with adverse outcomes, evaluated as death or ICU admission.

Alterations in coagulation parameters, in particular high DD level and low PLT, have been linked with severe COVID-19 patients (16,17). These disorders reflect the hypercoagulable state present in poor prognosis, which could promote microthrombosis in the lungs, as well as in other organs (18).

Elevated TNI levels are frequent in patients with COVID-19 and have been significantly associated with fatal outcomes. Several mechanisms may explain this phenomenon: viral myocarditis, cytokine-driven myocardial damage, microangiopathy, and unmasked coronary artery disease. SARS-CoV-2 uses angiotensin-converting enzyme 2 (ACE2) as its entry receptor and subsequently downregulates ACE2 expression. This mechanism may complicate the clinical course mediated through inflammatory response, endothelial dysfunction, and microvascular damage (19).

Early monitoring of immunological biomarkers is an important basis to guide treatment strategies in COVID-19. In this study, CRP was the only immunological biomarker assessed significantly related to mortality. Recently, a meta-analysis including 16 independent studies highlighted the importance of CRP as a possible biomarker for mortality due to COVID-19 infection (20). Furthermore, the study by Wang (21) showed that CRP levels were positively correlated with lung lesion and disease severity in the early stage of COVID-19.

Lymphopenia is a common feature in patients with COVID-19. Significant decreases in T-cell counts have been observed in patients with severe disease (22). Up to now, the underlying mechanisms leading to the observed lymphopenia are little known and better understanding will provide insight into better management of such patients (23).

A high serum CREA level is a frequently observed complication in nonsurvivor inpatients (24). It has been described that around 20% of patients admitted to an ICU require renal replacement therapy 15 days after illness onset (25).

Previous studies reported comorbidities to be one of the most important risk factors associated with increased disease severity (6,7,26). Likewise, our study reported a significant association between mortality and some of the collected comorbidities, including diabetes, dyslipidemia, hypertension, heart failure, and ischemic heart disease. Despite these differences found between survivors and nonsurvivors, none of our prediction models did include any comorbidity since the clinical laboratory measurements were stronger predictors of mortality in patients with COVID-19.

Age was the only nonlaboratory-related variable associated with symptom aggravation in our study. This is in accordance with previous publications reporting age to be the most important predictor of death in patients with COVID-19 (27). Immunosenescence is defined as the declined ability of elderly patients to react properly upon infection, to initiate and maintain an adequate protective immune response, and to develop immunological memory (28). Thus, the severity of viral infections (e.g., influenza, respiratory syncytial virus) is notably increased among older adults compared to younger individuals, and more acute and long-term sequelae often develop as a result (29,30).

Other studies have been published using machine learning models to predict the mortality in COVID-19 patients, and some of them were included in systematic reviews and meta-analysis (31). Our study presents some common points with these publications since the predictors used in the BGM score were also identified to be relevant predictors of mortality in other models, supporting their significant association with adverse patient outcomes. One of our study's strengths is that we have used a relatively large sample size compared with the research items cited in the meta-analysis, including a substantial number of nonsurvivors. Also, our final algorithm, the BGM score, only includes a small number of simple laboratory measurements, which makes our model easy to implement in the routine clinical practice. It's noteworthy that all the variables of our study were collected in the first 48 hours of admission. Hence, our model can provide an early detection of patients at high risk of death, favoring early interventions.

Our study has several limitations. First, it was a retrospective single-center study, which may lead to biased results. Second, we recruited only patients with moderate or severe-stage disease and not asymptomatic or mild-stage disease. Therefore, prospective multicenter studies including patients with various stages of disease are warranted to confirm the reliability of the BGM score model.

The effects the pandemic is causing on medical resources worldwide highlight the need to develop early predictor models capable of detecting which patients can be managed safely at district hospital or can benefit from domiciliary hospitalization programs and which ones will need intensive care. Therefore, identifying risk factors at presentation that predict the likelihood of disease progression will be useful to: (1) increase the therapeutic effect in patients with a risk of higher disease progression and (2) reduce the mean hospitalization time in patients not at risk.

To conclude, we have developed an easy-to-use model comprising biochemical, hematological, and coagulation parameters presented in most clinical laboratories able to predict the survival probability of a patient with COVID-19 with high accuracy. This web tool may support clinicians in managing this infectious disease and providing focused interventions to patients with COVID-19 at a higher risk of death.

Disclosures

References

1. The Lancet. Emerging understandings of 2019-nCoV. *Lancet*. 2020;395(10221):311. CrossRef PubMed
2. Zhu N, Zhang D, Wang W, et al; China Novel Coronavirus Investigating and Research Team. A novel coronavirus from patients with pneumonia in China, 2019. *N Engl J Med*. 2020;382(8): 727-733. CrossRef PubMed
3. World Health Organization. Report of the WHO-China Joint Mission on Coronavirus Disease 2019 (COVID-19). Online (Accessed September 2020).
4. European Centre for Disease Prevention and Control. Novel coronavirus disease 2019 (COVID-19) pandemic: increased transmission in the EU/EEA and the UK – sixth update. Online (Accessed September 2020).
5. Richardson S, Hirsch JS, Narasimhan M, et al; the Northwell COVID-19 Research Consortium. Presenting Characteristics, Comorbidities, and Outcomes Among 5700 Patients Hospitalized With COVID-19 in the New York City Area. *JAMA*. 2020;323(20):2052-2059. CrossRef PubMed
6. Chen N, Zhou M, Dong X, et al. Epidemiological and clinical characteristics of 99 cases of 2019 novel coronavirus pneumonia in Wuhan, China: a descriptive study. *Lancet*. 2020;395(10223):507-513. CrossRef PubMed
7. Wang D, Hu B, Hu C, et al. Clinical Characteristics of 138 Hospitalized Patients With 2019 Novel Coronavirus-Infected Pneumonia in Wuhan, China. *JAMA*. 2020;323(11):1061-1069. CrossRef PubMed
8. Hou H, Zhang B, Huang H, et al. Using IL-2R/lymphocytes for predicting the clinical progression of patients with COVID-19. *Clin Exp Immunol*. 2020;201(1):76-84. CrossRef PubMed
9. Shen B, Yi X, Sun Y, et al. Proteomic and Metabolomic Characterization of COVID-19 Patient Sera. *Cell*. 2020;182(1):59-72. e15. CrossRef PubMed
10. Messner CB, Demichev V, Wendisch D, et al. Ultra-High-Throughput Clinical Proteomics Reveals Classifiers of COVID-19 Infection. *Cell Syst*. 2020;11(1):11-24.e4. CrossRef PubMed
11. Kuhn M. caret: Classification and Regression Training. R package version 6.0-86; 2020. Online
12. Therneau T, Atkinson B, Ripley B, Ripley MB. rpart: Recursive Partitioning and Regression Trees. R Packag version 41-10; 2019. Online
13. Venables WN, Ripley BD. *Modern Applied Statistics With S*. 4th ed. New York: Springer; 2002. CrossRef
14. Chang W, Cheng J, Allaire J, Xie Y, McPherson J. shiny: Web Application Framework for R. R package version 1.5.0;2020. Online
15. Sisó-Almirall A, Kostov B, Mas-Heredia M, et al. Prognostic factors in Spanish COVID-19 patients: A case series from Barcelona. *PLoS One*. 2020;15(8):e0237960. CrossRef PubMed
16. Tang N, Li D, Wang X, Sun Z. Abnormal coagulation parameters are associated with poor prognosis in patients with novel coronavirus pneumonia. *J Thromb Haemost*. 2020;18(4):844-847. CrossRef PubMed
17. Lippi G, Plebani M, Henry BM. Thrombocytopenia is associated with severe coronavirus disease 2019 (COVID-19) infections: A meta-analysis. *Clin Chim Acta*. 2020;506:145-148. CrossRef PubMed
18. Salamanna F, Maglio M, Landini MP, Fini M. Platelet functions and activities as potential hematologic parameters

related to Coronavirus Disease 2019 (Covid-19). *Platelets*. 2020;31(5):627-632. CrossRef PubMed

19. Tersalvi G, Vicenzi M, Calabretta D, Biasco L, Pedrazzini G, Winterton D. Elevated Troponin in Patients With Coronavirus Disease 2019: possible Mechanisms. *J Card Fail*. 2020; 26(6):470-475. CrossRef PubMed

20. Sahu BR, Kampa RK, Padhi A, Panda AK. C-reactive protein: A promising biomarker for poor prognosis in COVID-19 infection. *Clin Chim Acta*. 2020;509:91-94. CrossRef PubMed

21. Wang L. C-reactive protein levels in the early stage of COVID-19. *Med Mal Infect*. 2020;50(4):332-334. CrossRef PubMed

22. Liu Z, Long W, Tu M, et al. Lymphocyte subset (CD4+, CD8+) counts reflect the severity of infection and predict the clinical outcomes in patients with COVID-19. *J Infect*. 2020;81(2): 318-356. CrossRef PubMed

23. Tavakolpour S, Rakhshandehroo T, Wei EX, Rashidian M. Lymphopenia during the COVID-19 infection: what it shows and what can be learned. *Immunol Lett*. 2020;225:31-32. CrossRef PubMed

24. Li Z, Wu M, Yao J, et al. Caution on Kidney Dysfunctions of COVID-19 Patients. Preprint Online (2020).

25. Zhou F, Yu T, Du R, et al. Clinical course and risk factors for mortality of adult inpatients with COVID-19 in Wuhan, China: a retrospective cohort study. *Lancet*. 2020;395(10229): 1054-1062. CrossRef PubMed

26. Chang MC, Park YK, Kim BO, Park D. Risk factors for disease progression in COVID-19 patients. *BMC Infect Dis*. 2020;20(1):445. CrossRef PubMed

27. Porcheddu R, Serra C, Kelvin D, Kelvin N, Rubino S. Similarity in Case Fatality Rates (CFR) of COVID-19/SARS-COV-2 in Italy and China. *J Infect Dev Ctries*. 2020;14(2):125-128. CrossRef PubMed

28. Reber AJ, Chirkova T, Kim JH, et al. Immunosenescence and challenges of vaccination against influenza in the aging population. *Aging Dis*. 2012;3(1):68-90. PubMed

29. Gordon A, Reingold A. The Burden of Influenza: a Complex Problem. *Curr Epidemiol Rep*. 2018;5(1):1-9. CrossRef PubMed

30. Gozalo PL, Pop-Vicas A, Feng Z, Gravenstein S, Mor V. Effect of influenza on functional decline. *J Am Geriatr Soc*. 2012;60(7):1260-1267. CrossRef PubMed

31. Wynants L, Van Calster B, Collins GS, et al. Prediction models for diagnosis and prognosis of covid-19 infection: systematic review and critical appraisal. *BMJ*. 2020;369:m1328. CrossRef PubMed

Circulating progastrin-releasing peptide in the diagnosis of Small Cell Lung Cancer (SCLC) and in therapeutic monitoring

Vittoria Barchiesi[1], Vittorio Simeon[2], Claudia Sandomenico[3], Monica Cantile[4], Dionigio Cerasuolo[5], Paolo Chiodini[2], Alessandro Morabito[3], Ernesta Cavalcanti[5]

[1]Department "Campania Centro", A.O.R.N. "Antonio Cardarelli", Napoli - Italy
[2]Medical Statistics Unit, University of Campania "Luigi Vanvitelli", Napoli - Italy
[3]Thoracic Medical Oncology Unit, Istituto Nazionale Tumori IRCCS, "Fondazione G.Pascale", Napoli - Italy
[4]Pathology Unit, Istituto Nazionale Tumori IRCCS, "Fondazione G.Pascale", Napoli - Italy
[5]Laboratory Medicine Unit, Istituto Nazionale Tumori IRCCS, "Fondazione G.Pascale", Napoli - Italy

ABSTRACT

Introduction: Progastrin-releasing peptide (proGRP), a precursor of GRP, has been recently reported as a putative circulating biomarker for differential diagnosis between non–small cell lung cancer (NSCLC) and SCLC. We evaluated the diagnostic effectiveness of proGRP to differentiate patients with NSCLC and SCLC and the usefulness of combined measurement of proGRP and neuron-specific enolase (NSE) for diagnosing SCLC.
Methods: Serum proGRP, NSE, cytokeratin 19 fragment 21-1 (CYFRA 21.1), squamous cell carcinoma antigen (SCC Ag) and carcinoembryonic antigen (CEA) were prospectively collected and measured in patients with a new diagnosis of lung cancer. Serum proGRP was also measured in healthy subjects. The serum proGRP, NSE, CYFRA 21.1 and CEA concentrations were determined by an electrochemiluminescence immunoassay and the serum SCC Ag concentration was determined by an automated immunofluorescence assay. Differences between proGRP and NSE in patients with SCLC and NSCLC were evaluated and compared using Mann-Whitney test.
Results: A total of 77 patients affected by SCLC (n = 17) and NSCLC (n = 60) were enrolled in the present study. Moreover, 50 cases of healthy subjects were analyzed for proGRP. SCLC patients showed a significantly higher proGRP (1,484 pg/mL; range 168-3,777) levels compared to NSCLC patients (45 pg/mL; range 31.7-60.6), p<0.0001. In healthy subjects the median proGRP level was 36.1 (28.8-43.5) pg/mL, significantly lower than SCLC patients. ProGRP showed a higher specificity when compared to NSE, with a difference in proportion of 47.5% (95% confidence interval 32.5% to 62.5%, p<0.001). Serial measurements of proGRP in SCLC patients showed a decrease in responsive chemotherapy patients.
Conclusions: ProGRP is an accurate biomarker for diagnosis of SCLC and for discrimination of SCLC from NSCLC.

Keywords: Lung cancer, proGRP, Serum biomarker

Introduction

Lung cancer is one of the most common and malignant tumors, with high morbidity and mortality worldwide, and its incidence has been increasing, especially among women, in the last decades (1,2). The early diagnosis and accurate staging of lung cancer for immediate and appropriate treatment are among the main strategies to improve survival rates (3). The first step in the diagnosis is to distinguish between non–small cell lung cancer (NSCLC) and SCLC, which has a poorer prognosis (4,5). Despite lung cancer diagnosis being only based on histology, different serum biomarkers have been proven to be useful tools for the diagnosis, prognosis and follow-up, but there are currently no guidelines or standards on their application in clinical practice (6,7). The National Academy of Clinical Biochemistry (NACB) Laboratory Medicine Practice Guidelines (8) recommend carcinoembryonic antigen (CEA), squamous cell carcinoma–related antigen (SCC-Ag), neuron-specific enolase (NSE), cytokeratin 19 fragment 21-1 (CYFRA 21.1), carbohydrate antigen 125 (CA 125) and progastrin-releasing peptide (proGRP) as routine markers of lung cancer. NSE is considered the tumor marker of choice in SCLC diagnosis, but it is not pathognomonic because its effectiveness is related to the stage of the tumor (9).

ProGRP is a precursor of gastrin-releasing peptide (GRP), an active hormone involved in the physiological digestive process. GRP is a 27-amino-acid peptide homologous to the C-terminal of bombesin isolated from porcine stomach, in fetal as well as neonatal lung tissue and in primary lung cancer, particularly in SCLC (10-13).

GRP cannot be used as a biomarker due to its instability (half-life of GRP is 2 min), while proGRP is a stable protein with a half-life of 19-28 days. Recently, circulating proGRP has been reported as a putative biomarker for differential diagnosis between NSCLC and SCLC (14-18).

The aim of the present study was to evaluate the diagnostic effectiveness of proGRP to differentiate patients with NSCLC and SCLC, the usefulness of combined measurement of proGRP and NSE for the diagnosis of SCLC, the comparison of diagnostic efficacy of proGRP vs. a combined panel of tumor markers and to establish the reference values of proGRP in healthy patients.

Methods

Patients

Serum proGRP, NSE, CYFRA 21.1, SCC Ag and CEA were prospectively collected and measured in patients with a new diagnosis of lung cancer admitted to the Thoracic Medical Oncology of the National Cancer Institute "G. Pascale" of Naples.

Moreover, serum proGRP was measured in healthy subjects collected at the Unit of Transfusional Medicine of the National Cancer Institute "G. Pascale" of Naples.

The present study was approved through the Ethics Committee and all patients completed an informed consent.

Assay

Serum samples were taken in Vacutainer tube SST II Advance and analyzed in less than 1 hour. Serum proGRP, NSE, CYFRA 21.1 and CEA concentrations were determined by an electrochemiluminescence immunoassay on a Cobas C6000 automated analyzer (Roche Diagnostics). Serum SCC Ag concentration was determined by an automated immunofluorescence assay on Kryptor compact plus (Thermo Scientific). For all analytes the reference range was set according to the data sheet manufacturer.

Statistical Analysis

Data were described as reported: continuous variables as mean and standard deviation, or median and interquartile range if distribution was not symmetric; categorical variables as number and percentage. Differences of diagnostic markers proGRP and NSE in patients with SCLC and NSCLC were evaluated and compared using Mann-Whitney test. Successively, proGRP and NSE were categorized and defined positive using these criteria: cutoff >100 pg/mL for proGRP; >17 ng/mL for NSE. Furthermore, the algorithm proposed by Molina et al. (19), taking into consideration SCC, proGRP, NSE, CYFRA and CEA, was used to classify patients. For each biomarker (proGRP, NSE and algorithm), the diagnostic measures, such as sensitivity, specificity, positive predictive value (PPV) and negative predictive value (NPV), were calculated to evaluate the accuracy in discriminating SCLC from NSCLC. Pairwise comparison of diagnostic measures was performed using McNemar's test (20). Receiver operating characteristic (ROC) curve analysis was calculated to define new threshold values for proGRP and NSE in our population. The area under the ROC curve (AUC) was used to quantify accuracy and define sensitivity and specificity. For descriptive purpose, proGRP values (in log scale) in SCLC patients were collected and reported for the whole treatment period. All tests were two-tailed and a p-value <0.05 was considered statistically significant. All data were analyzed using R software 3.3.1 (R foundation for Statistical Computing, Vienna, Austria).

Results

ProGRP serum level in lung cancer patients

A total of 77 patients affected by lung cancer, 17 SCLC and 60 NSCLC, were enrolled in the present study between July 2015 and July 2017; moreover, 50 cases of healthy subjects were collected from the Unit of Transfusional Medicine, at the National Cancer Institute "G. Pascale" of Naples, Italy.

The study design is shown in Figure 1.

The mean age of the 17 SCLC patients was 63.4 ± 8.6 years and there were 10 (58.8%) male and 7 (41.2%) female patients. The 60 NSCLC patients were older (68.4 ± 9.1 years) and with higher proportion of male patients (65%) (Tab. I).

The median (interquartile range [IQR]) proGRP level in the total population was 47.3 (34.3-87.3) pg/mL. SCLC patients showed (Tab. I and Fig. 2) a significantly higher proGRP (1,484 [168-3,777] pg/mL] levels compared to NSCLC patients (45 [31.7-60.6] pg/mL) (Mann-Whitney test, p<0.0001). In addition, NSE was significantly higher in SCLC than NSCLC patients
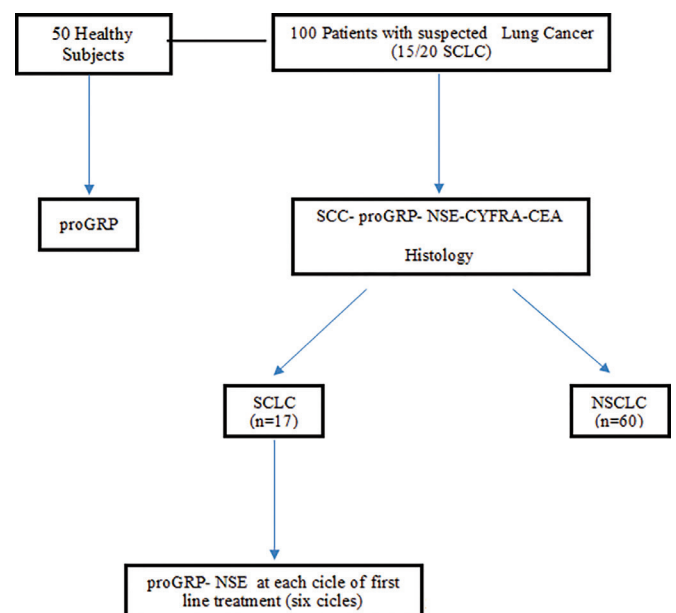
Fig. 1 - Flow chart of the study design.

TABLE I - Patients' characteristics and values of different analytes

	Total patients (n = 77)	SCLC (n = 17, 22%)	NSCLC (n = 60, 78%)
Age, years			
Mean (SD)	67.3 (9.16)	63.4 (8.6)	68.4 (9.11)
Sex, n (%)			
Female	28 (36.40)	7 (41.2)	21 (35.00)
Male	49 (66.60)	10 (58.8)	39 (65.00)
Creatinine, mg/dL			
Median (IQR)	0.82 (0.67-0.93)	0.82 (0.68-0.9)	0.82 (0.66-0.96)
LDH, U/L			
Median (IQR)	418 (336-560)	510 (376-633)	415 (330-543)
AST, U/L			
Median (IQR)	17 (13-22)	17 (13-22.5)	17 (14-22)
ALT, U/L			
Median (IQR)	16 (12-25)	16 (11-20)	16 (12-26)
Bilirubin, mg/dL			
Median (IQR)	0.5 (0.4-0.7)	0.5 (0.4-0.6)	0.5 (0.4-0.7)
CEA, ng/mL			
Median (IQR)	7.9 (3.1-38.9)	4.6 (3-17.9)	8.7 (3-42.6)
CYFRA, ng/mL			
Median (IQR)	5.4 (3.2-12.7)	3.4 (2.3-6.4)	7 (3.3-13.7)
NSE, ng/mL			
Median (IQR)	19 (14.2-27.6)	55 (34-107.4)	17.7 (13-24)
SCC, ng/mL			
Median (IQR)	0.5 (0.1-0.8)	0.2 (0.1-0.6)	0.5 (0.2-1.1)
proGRP, pg/mL			
Median (IQR)	47.3 (34.3-87.3)	1484 (168-3777)	45 (31.7-60.6)
proGRP (log10)			
Mean (SD)	1.9 (0.8)	3 (1)	1.7 (0.3)

ALT = alanine aminotransferase; AST = aspartate transaminase; CEA = carcinoembryonic antigen; CYFRA 21.1 = cytokeratin 19 fragment 21-1; IQR = interquartile range; LDH = lactate dehydrogenase; NSCLC = non–small cell lung cancer; NSE = neuron-specific enolase; proGRP = precursor of gastrin-releasing peptide; SCC = squamous cell carcinoma; SCLC = small cell lung cancer; SD = standard deviation.

(55 [34-107.4] ng/mL versus 17.7 [13-24] ng/mL), whereas CYFRA 21.1 was lower in SCLC patients. There were no differences for CEA and SCC biomarkers.

In healthy subjects the median proGRP level was 36.1 (28.8-43.5) pg/mL, significantly lower than SCLC patients (data not shown).

ProGRP and NSE in lung cancer histological types and therapeutic response

Diagnostic accuracy of each biomarker is reported in Table II. According to lung cancer histological type, proGRP showed a sensitivity of 82.4% (95% confidence interval [CI], 56.6-96.2) with a specificity of 93.3% (95% CI, 83.8-98.2). PPV and NPV were 77.8% and 94.9%, respectively. NSE biomarker and algorithm (NSE + proGRP) showed the following value of accuracy: sensitivity (100% and 86.7%, respectively), specificity (45% and 96.6%, respectively), PPV (34% and 86.7%, respectively) and NPV (100% and 96.6%, respectively). Pairwise comparison of proGRP with NSE and algorithm highlighted no differences in terms of sensitivity. ProGRP showed a higher specificity when compared to NSE, with a difference in proportion of 47.5% (95% CI 32.5% to 62.5%, Exact McNemar's test p<0.001). ProGRP and algorithm measures revealed a similar performance for both of them.

On ROC curve analysis, AUC for proGRP and NSE was comparable with 0.86 (95% CI, 0.71-1) and 0.92 (95% CI, 0.84-0.99), respectively (Fig. 3).

Serial measurements of proGRP in 12 SCLC patients showed a decrease in responsive patients and they are depicted in Figure 4.

Discussion

In our study, median proGRP levels were significantly higher in patients with SCLC than in those with NSCLC or healthy subjects. Plasma proGRP at cutoff level of 100 pg/mL showed a high sensitivity and specificity (82.4% and 93.3%, respectively) in identifying patients with SCLC, with a specificity higher than NSE. PPV and NPV were 77.8% and 94.9%, respectively. Moreover, responsive patients presented a decrease in proGRP levels. These results confirm the accuracy of proGRP in clinical practice in the diagnosis of SCLC.

In 2011, a meta-analysis of 5,146 patients enrolled in 11 clinical trials, including 1,095 with SCLC, concluded that
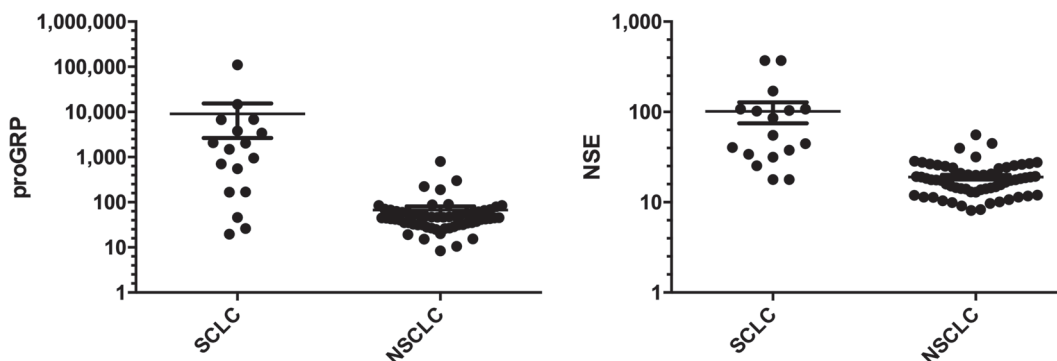
Fig. 2 - ProGRP and NSE levels in SCLC and NSCLC. On the left: proGRP level in SCLC and NSCLC patients; on the right: NSE level in SCLC and NSCLC patients. NSCLC = non-small-cell lung cancer; NSE = neuron-specific enolase; proGRP = progastrin-releasing peptide; SCLC = small cell lung cancer. Values were reported in log10 scale.

TABLE II - Diagnostic accuracy of proGRP, NSE and their combination in discriminating SCLC from NSCLC

	Sn	Sp	PPV	NPV
proGRP	82.4 (56.6-96.2)	93.3 (83.8-98.2)	77.8 (52.4-93.6)	94.9 (85.9-98.9)
NSE	100 (80.5-99.9)	45 (32.1-58.4)*	34 (21.2-48.8)	100 (87.2-100)
Algorithm	86.7 (59.5-98.3)	96.6 (88.3-99.6)	86.7 (59.5-98.3)	96.6 (88.3-99.6)

NPV = negative predictive value; NSE = neuron-specific enolase; PPV = positive predictive value; proGRP = progastrin-releasing peptide; Sn = sensitivity; Sp = specificity.
*Exact McNemar's test p<0.001.
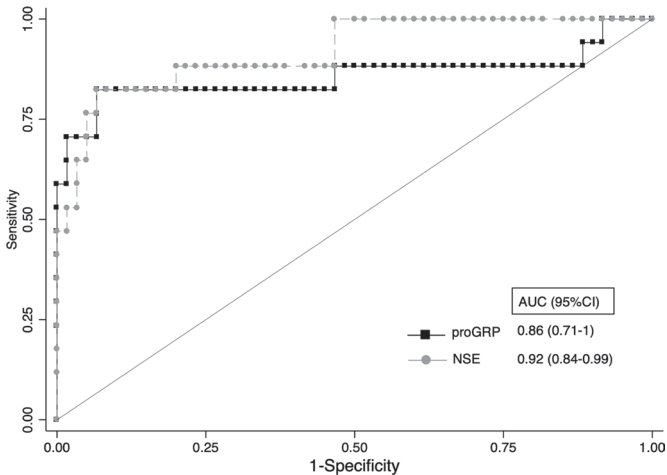
Fig. 3 - Receiver operating characteristics (ROC) curves of proGRP and NSE. NSE = neuron-specific enolase; proGRP = progastrin-releasing peptide. Area under the curve (AUC) were reported.
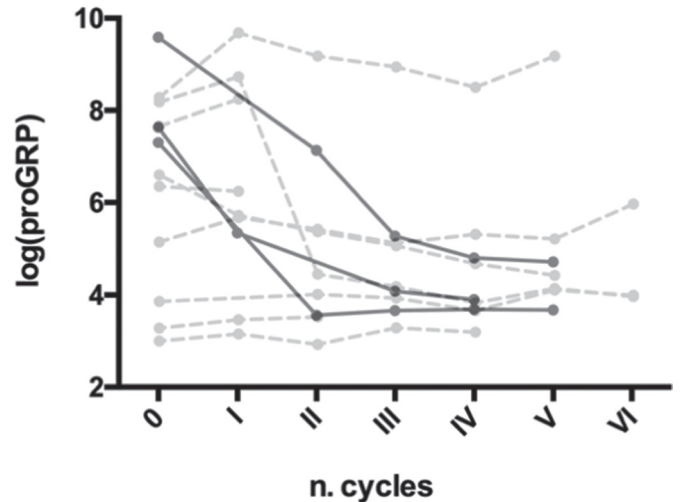
Fig. 4 - Serial measurement of proGRP in SCLC patients and correlation with therapeutic response. Black point with solid line describes patients with complete response to therapy. Gray point with dashed line describes patients with partial response to therapy. proGRP = progastrin-releasing peptide; SCLC = small cell lung cancer.

proGRP appeared to be a promising marker for SCLC, with a sensitivity of 71.6% and a specificity of 92.1% (21). However, the poor pooled estimates of sensitivity, the wide range of sensitivity and specificity estimates across studies and the high degree of inconsistency made the conclusions of the meta-analysis weak.

The levels of six tumor markers, CYFRA21-1, CEA, NSE, CA125, proGRP and SCC, were evaluated in 392 Chinese patients affected by lung cancer (including 308 with NSCLC and 84 with SCLC), in 116 patients with benign lung diseases and in 144 healthy controls (22). The results showed that the levels of NSE and proGRP were significantly higher in the SCLC group than in the NSCLC group and that the sensitivity (at 95% specificity) of NSE, proGRP and the combination of the two markers for differential diagnosis of NSCLC and SCLC was 71.9%, 90.6% and 90.8%, respectively.

In a Chinese study, plasma proGRP levels were prospectively measured in 75 SCLC patients, and they were significantly higher than those of 234 NSCLC patients (1058.0 vs. 37.46 pg/mL, p<0.001) (23). In this study, proGRP showed 87.8% sensitivity and 91.5% specificity, at a cutoff level of 65.7 pg/mL. Moreover, change of proGRP levels before and after chemotherapy was analyzed. In patients with SCLC who were followed through the treatment, the median proGRP levels of the responders decreased after chemotherapy (p<0.001).

A retrospective Italian study evaluated serum proGRP levels in 37 patients with SCLC and 28 patients with advanced NSCLC (24). Median proGRP level was 919 pg/mL in SCLC

and 32 pg/mL in NSCLC (p<0.0001). In this study, proGRP showed 86.4% sensitivity and 96.4% specificity, at a cutoff level of 77.8 pg/mL. Moreover, in patients with extended disease, median proGRP was 46-fold higher than in patients with limited disease (p = 0.004), notwithstanding all the limitations of a statistical analysis conducted over a small-size population.

The results of our study support the use of proGRP at diagnosis to discriminate SCLC from NSCLC or nonmalignant disease. Strengths of our analysis are the prospective design of the study and the inclusion also of health controls to determine the reference values of proGRP in healthy subjects, not evaluated to date in other studies. Furthermore, our study highlights that the diagnostic efficiency of the test is equivalent to that demonstrated by the association of tests included in the diagnostic algorithms, suggesting that proGRP can be considered a valid test to reduce time and costs.

Limitations of our study are the small number of patients enrolled in the study and, in particular, of those with SCLC evaluated with serial measurements of proGRP during treatment. A larger study to confirm the predictive role of proGRP reduction in early identification of responsive SCLC patients to first-line treatment with chemotherapy combined with immunotherapy is planned.

In conclusion, proGRP is an accurate biomarker for the diagnosis of SCLC and for discriminating SCLC from NSCLC.

Further studies should confirm its utility also for treatment and monitoring of SCLC patients.

Abbreviations

AUC = area under the curve; CEA = carcinoembryonic antigen; CYFRA 21.1 = cytokeratin 19 fragment 21-1; GRP = gastrin-releasing peptide; IQR = interquartile range; NACB = National Academy of Clinical Biochemistry; NPV = negative predictive value; NSCLC = non–small cell lung cancer; NSE = neuron-specific enolase; PPV = positive predictive value; proGRP = precursor of gastrin-releasing peptide; ROC = receiver operating characteristics; SCC Ag = squamous cell carcinoma antigen; SCLC = small cell lung cancer.

Acknowledgments

Data Availability

The data that support the findings of this study are available from the corresponding author on reasonable request.

Disclosures

References

1. Ferlay J, Soerjomataram I, Dikshit R, et al. Cancer incidence and mortality worldwide: sources, methods and major patterns in GLOBOCAN 2012. Int J Cancer. 2015;136(5):E359-E386. CrossRef PubMed
2. Siegel RL, Miller KD, Jemal A. Cancer statistics, 2016. CA Cancer J Clin. 2016;66(1):7-30. CrossRef PubMed
3. Currie GP, Kennedy AM, Denison AR. Tools used in the diagnosis and staging of lung cancer: what's old and what's new? QJM. 2009;102(7):443-448. CrossRef PubMed
4. NCCN Clinical Practice Guidelines in Oncology. Non-small cell lung cancer. V6. Online (Accessed: October 2020).
5. Byers LA, Rudin CM. Small cell lung cancer: where do we go from here? Cancer. 2015;121(5):664-672. CrossRef PubMed
6. Dong Y, Zheng X, Yang Z, et al. Serum carcinoembryonic antigen, neuron-specific enolase as biomarkers for diagnosis of nonsmall cell lung cancer. J Cancer Res Ther. 2016;12(5)(suppl):34-36. CrossRef PubMed
7. Molina R, Augé JM, Bosch X, et al. Usefulness of serum tumor markers, including progastrin-releasing peptide, in patients with lung cancer: correlation with histology. Tumour Biol. 2009;30(3):121-129. CrossRef PubMed
8. NACB: Practice Guidelines and Recommendations for use of Tumor Markers in the Clinic Lung Cancer (Section 3P), 2006.
9. Molina R, Holdenrieder S, Auge JM, Schalhorn A, Hatz R, Stieber P. Diagnostic relevance of circulating biomarkers in patients with lung cancer. Cancer Biomark. 2010;6(3-4):163-178. CrossRef PubMed
10. Yamaguchi K, Abe K, Kameya T, et al. Production and molecular size heterogeneity of immunoreactive gastrin-releasing peptide in fetal and adult lungs and primary lung tumors. Cancer Res. 1983;43(8):3932-3939. PubMed
11. Wang D, Yeger H, Cutz E. Expression of gastrin-releasing peptide receptor gene in developing lung. Am J Respir Cell Mol Biol. 1996;14(5):409-416. CrossRef PubMed
12. Erisman MD, Linnoila RI, Hernandez O, DiAugustine RP, Lazarus LH. Human lung small-cell carcinoma contains bombesin. Proc Natl Acad Sci USA. 1982;79(7):2379-2383. CrossRef PubMed
13. Moody TW, Pert CB, Gazdar AF, Carney DN, Minna JD. High levels of intracellular bombesin characterize human small-cell lung carcinoma. Science. 1981;214(4526):1246-1248. CrossRef PubMed
14. Lv ShP, Wang Y, Huang L, Wang F, Zhou JG, Ma H. Meta-analysis of serum gastrin-releasing peptide precursor as a biomarker for diagnosis of small cell lung cancer. Asian Pac J Cancer Prev. 2017;18(2):391-397. PubMed
15. Holdenrieder S, von Pawel J, Dankelmann E, et al. Nucleosomes, ProGRP, NSE, CYFRA 21-1, and CEA in monitoring first-line chemotherapy of small cell lung cancer. Clin Cancer Res. 2008;14(23):7813-7821. CrossRef PubMed
16. Wojcik E, Kulpa JK. Pro-gastrin-releasing peptide (ProGRP) as a biomarker in small-cell lung cancer diagnosis, monitoring and evaluation of treatment response. Lung Cancer (Auckl). 2017;8:231-240. CrossRef PubMed
17. Kim HR, Oh IJ, Shin MG, et al. Plasma proGRP concentration is sensitive and specific for discriminating small cell lung cancer from nonmalignant conditions or non-small cell lung cancer. J Korean Med Sci. 2011;26(5):625-630. CrossRef PubMed
18. Oh HJ, Park HY, Kim KH, et al. Progastrin-releasing peptide as a diagnostic and therapeutic biomarker of small cell lung cancer. J Thorac Dis. 2016;8(9):2530-2537. CrossRef PubMed
19. Molina R, Auge JM, Filella X, et al. Pro-gastrin-releasing peptide (proGRP) in patients with benign and malignant diseases: comparison with CEA, SCC, CYFRA 21-1 and NSE in patients with lung cancer. Anticancer Res. 2005;25(3A):1773-1778. PubMed
20. Zhou X, Obuchowski N, McClish D. Comparing the accuracy of two diagnostic tests. 2nd ed. Statistical methods in diagnostic medicine. Wiley 2011. CrossRef
21. Yang HJ, Gu Y, Chen C, Xu C, Bao YX. Diagnostic value of pro-gastrin-releasing peptide for small cell lung cancer: a meta-analysis. Clin Chem Lab Med. 2011;49(6):1039-1046. CrossRef PubMed
22. Wang L, Wang D, Zheng G, et al. Clinical evaluation and therapeutic monitoring value of serum tumor markers in lung cancer. Int J Biol Markers. 2016;31(1):e80-e87. CrossRef PubMed
23. Wu XY, Hu YB, Li HJ, et al. Diagnostic and therapeutic value of progastrin-releasing peptide on small-cell lung cancer: a single-center experience in China. J Cell Mol Med. 2018;22(9):4328-4334. CrossRef PubMed
24. Cavalieri S, Morelli D, Martinetti A, et al. Clinical implications for pro-GRP in small cell lung cancer. A single center experience. Int J Biol Markers. 2018;33(1):55-61. CrossRef PubMed

Circulating erythroblast abnormality associated with systemic pathologies may indicate bone marrow damage

Stefan Schreier[1-3], Prapaphan Budchart[3], Suparerk Borwornpinyo[3,4], Wichit Arpornwirat[5], Wannapong Triampo[2,6]

[1]School of Bioinnovation and Bio-based Product Intelligence, Faculty of Science, Mahidol University, Rama VI Rd, Bangkok - Thailand
[2]Thailand Center of Excellence in Physics, Ministry of Higher Education, Science, Research and Innovation, Bangkok - Thailand
[3]Premise Biosystems Co., Ltd. Bangkok - Thailand
[4]Excellent Center for Drug Discovery, Faculty of Science, Mahidol University, Rama VI, Rd, Bangkok - Thailand
[5]Department of Oncology, Bangkok Hospital, Bangkok - Thailand
[6]Department of Physics, Faculty of Science, Mahidol University, Bangkok - Thailand

ABSTRACT

Background: The circulating rare cell population is diverse and rich in diagnostic information. Its characterization and clinical exploitation by cell-based liquid biopsy is an ongoing research task. Bone marrow is one of the major contributors to the peripheral blood rare cell population and, consequently, determines individual rare cell profiles thus depending on bone marrow health status. Bone marrow damage has been associated with aggressive or late-stage systemic diseases and egress of various bone marrow cells into the blood circulation. The association of quantity and heterogeneity of circulating erythroblast with bone marrow damage is of particular interest.
Methods: Circulating CD71^{high}/CD45-/Hoechst^{high} blast cells from healthy, noncancer- and cancer-afflicted donors were enriched by CD45 depletion and analyzed by immunofluorescence microscopy.
Results: A new finding of aberrant and mitotic circulating erythroid-like cells that appear similar across blood donors afflicted with various systemic pathologies is reported. Further presented is a classification of said erythroblast-like cells in nine subcategories according to morphological differences between phenotypically similar cells.
Conclusion: Aberrant and mitotic bone marrow-derived rare circulating erythroid-like cells can be detected in the blood of afflicted individuals but not in healthy donors, suggesting the cause of bone marrow damage.

Keywords: Bone cancer, Bone marrow damage, Circulating rare cells, Erythroblast, Liquid biopsy

Introduction

Advancement in cell-based liquid biopsy (cbLB) comprises aspects of technology and biology (1,2). The latter often focused on the clinical translation of biomarkers mostly comprising known phenotypically specified cell types, such as epithelial, endothelial, or mesenchymal cells (3-5). A new chapter may have been opened with the awareness of the so-called circulating rare cell population (CRP) that holds the potential of cell discovery as well as of comprehensive cell analysis similar to a cytological investigation (6). CRP includes all kinds of non-hematopoietic but also rare hematopoietic

mainly bone marrow-derived cells and suggests a greater influence of bone marrow health status on individual CRP profiles and, most likely, vice versa. Conversely, high diagnostic potential of the CRP, in particular for the assessment of bone marrow damage (BMD), can be deduced yet still, which entails a steep gain in knowledge about character and functionality of individual rare cells (7). One of the most promising markers to be associated with BMD is the circulating erythroblast (CEB). This cell type is a known and common part of the CRP, yet has been rarely investigated for clinical applications in cbLB (6). We have earlier reported on the occurrence of immature CEB-like cells in healthy donors and suggested the association of respective findings above baseline with underlying pathologies affecting the bone marrow (8). Our data presented support of the hypothesis that increased levels of CEB predict BMD caused by chronic and systemic diseases. We herein report a new finding of erythroid cell abnormality with respect to poly-nucleation, cell pairing, and aggregation in association with systemic pathologies. The implications of the findings of, in particular, morphologically aberrant CEB would represent cytological evidence of BMD and be far-reaching for care in systemic diseases, for example, for the evidence-based prediction of distant invasion in cancer. As a first step into this research, we intend to describe

and classify the newly found CEB abnormalities as part of CRP associated with systemic disorders and provide first-hand evidence of the association with BMD.

Theory of liquid biopsy-based BMD detection

In cancer, BMD is an expected consequence of invasion by aggressive tumor cells referred to as disseminated tumor cells (DTC) and may entail a systemic response by way of egress of bone marrow cellular components that forms abnormal CRP profiles (6). Consequently, BMD detection in the setting of a cancer diagnosis is predictive of aggressive distant invasive disease. Relevant circulating cell types being indicative of and highly sensitive to slightest BMD are erythroid precursors that vary in quantity and maturation state upon bone marrow imbalances (8). CEB concentrations may vary in the range of <1 to 2×10^5 cells/mL depending on age, lifestyle in the lower concentration regimen, and disease type and severity in the higher concentration regimen, respectively. The pathological mechanism behind erythroblast egress as well as abnormalities is not well understood in particular for non-erythroid pathologies. We suggest at least two pathologies at work. One is the dysregulation of erythropoiesis, another is a dysfunctional blood barrier. We theorize that a change in the micro-environment of the so-called erythroid islands (9) at the vascular niche is caused by stress, for example, by invasion and nesting of aggressive DTC. Stress may be caused by inducing hypoxic conditions or by interaction with the erythroblast committed central macrophage or the erythroblasts themselves (10,11). Hypoxia develops in growing tumors, suggesting that active/aggressive DTC may induce hypoxia in the bone marrow micro-environment as well and may outstrip their ability to take up oxygen and nutrients from their environment by diffusion. Tumor-induced hypoxia is associated with poor prognosis (12). Furthermore, DTC are theorized to be in competition with erythroblasts for physical interaction with the central macrophage, and then changing the activation state of the central macrophage in the erythroid island most likely causing inflammatory cell recruitment, dysregulation of erythroblast proliferation and maturation, and destabilization of the vascular integrity. Furthermore, erythroblast cell cycle defects may be caused by altered mitochondrial function (13).

Methods

Patient cases

Nonspecific systemic pathologies were chosen to investigate the presence of CEB abnormality comprising a late- and early-stage breast cancer sample taking liquid biopsy before palliative treatment and after surgery and during chemoadjuvant therapy treatment, respectively. The collection further comprised an extensive stage small cell lung cancer (SCLC) patient taking a liquid biopsy during 3rd line chemotherapy therapy and a stage 4 non-small cell lung adenocarcinoma before palliative treatment. Another liquid biopsy was taken from a stage 3 head and neck cancer patient during chemotherapy. Furthermore, subjectively healthy persons with

known underlying pathologies included three individuals afflicted with diabetes type II, osteoporosis, and thrombocytosis, respectively. Informed consent was sought from the patient at the time of the blood draw in accordance with institutional review board (IRB) protocol.

Detection platform

The cbLB procedure has been described in our previous publication with modifications (8). In brief, 5 mL blood taken from 17 healthy donors and 4 cancer patients was subjected to pre-enrichment by red blood cell lysis yielding highly purified nucleated cells in the range of 1.8e7 to 5.5e7 cells. The cell suspension was further enriched by CD45 depletion assay employing an automated magnetic cell enrichment platform (Walderbach I, SanoLibio GmbH, Muenchen). The resulting cell suspension comprised carry-over leukocytes counting 3000 cells on average and all sorts of CD45-negative rare cells, among them CEB. In order to visualize their presence, the enriched cell suspension was subjected to cell membrane staining by conjugate antibodies reactive against CD71 and CD45 in both cases and nucleus staining by Hoechst Blue DNA stain. For analysis, the sample suspensions were loaded into a 386-well plate suitable for high-resolution image recording at 40× magnification using the Operetta system (PerkinElmar) and recording a bright field channel, channels for UV, green, and yellow fluorescence emission. Columbus analysis software served as screening and image analysis tool. Cells were identified as CEB in case of high expression of CD71 along the membrane, high nucleus density as well as complete absence of CD45 marker signal.

Results

We have identified known but also thus far unreported CEB morphologies exclusively in diseased individuals that follow in principle typical descriptions of erythroblast morphology and erythroid-specific CD71^{High}/CD45-/Hoechst^{High} phenotype. Detected cell morphologies could be recognized across diseases and therefore grouped into four main morphological distinct types which could be further divided into a total of nine subtypes (Fig. 1). Type 1 CEB represents normal erythroblasts and were found commonly in healthy donor blood at low concentrations, which can be further grouped into small (type 1a) and large (type 1b) erythroblasts owing to the size differences to the erythroblast maturation process (8). Type 1a is the most abundant cell type in all samples and represents the matured circulating counterpart of otherwise bone marrow dwelling orthochromatic erythroblasts with diameters in the range of 6.5 μm to about 12.4 μm. Type 1a cells corresponded to the commonly described appearance with dense nuclei and a high nucleus to cytoplasm ratio (N/C ratio). Class 1b denotes less frequent large CEB with diameters exceeding 12.4 μm as previously described (8). Apart from the size, immaturity is represented by a low-density chromatin nuclei in the diameter of about 6 μm to 10 μm and exhibiting a low N/C. Type 1 CEB may reflect abnormal erythropoiesis by cell elevation above normal concentrations only (Tab. I). Type 1 CEB could be further divided into subtypes 1c and 1d comprising
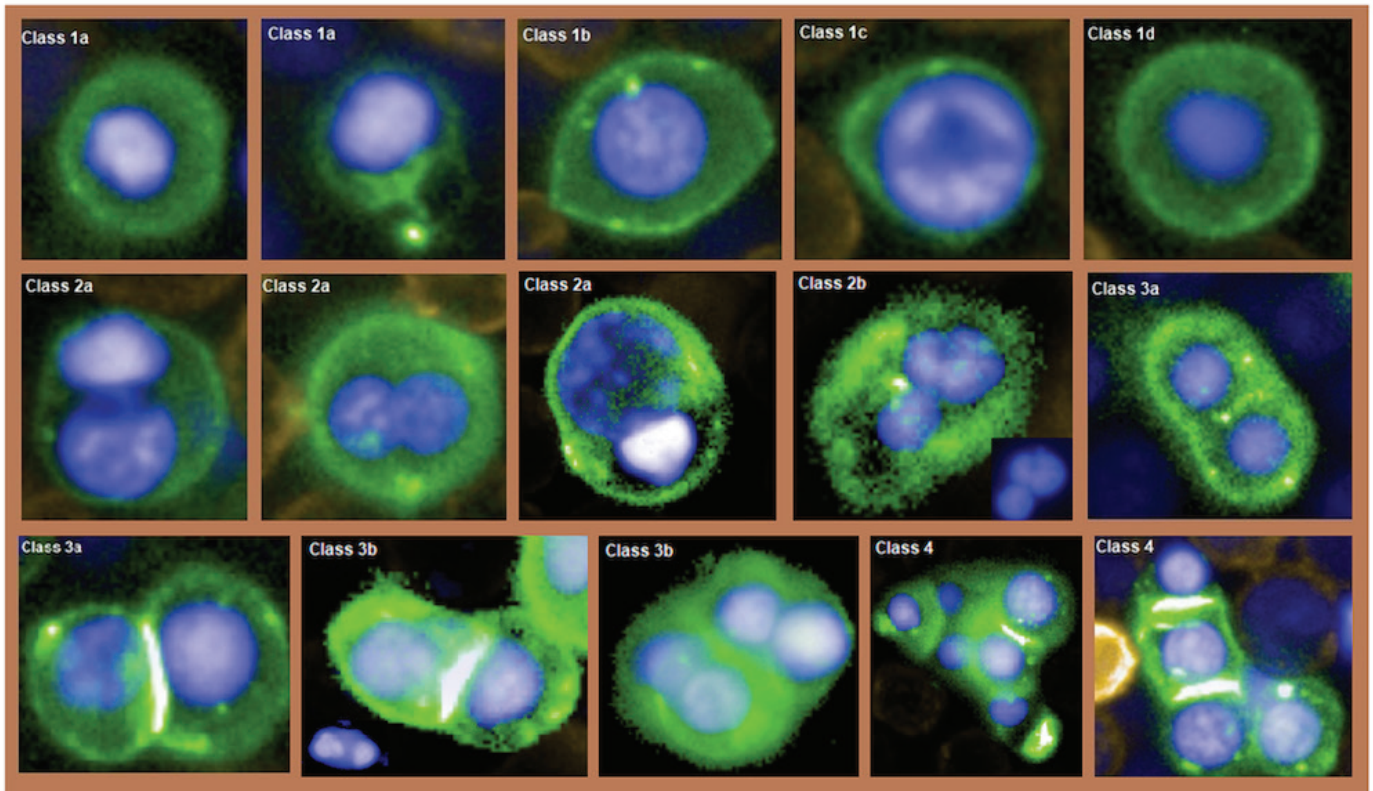
Fig. 1 - Gallery of CD71^{high}/CD45-/Hoechst^{high} circulating erythroblast (CEB) types. From left to right and upper to lower. The first two images represent normal erythroblasts measuring 10.5 μm and 7 μm in diameter, respectively. Next is shown a class 1b large CEB with low chromatin density measuring 14 μm in major diameter. Next is shown a megaloblast presenting irregular chromatin texture and is followed by a macro-normoblast. The following two images represent symmetric type 2a binucleated CEB. The next image represents an asymmetric aberrant type 2a binucleated CEB. Next is shown a type 2b CEB and is characteristic of a binucleated and multilobulated nucleus. The next two images represent symmetric mitotic CEB of class 3a. Next is shown a type 3b mitotic CEB with apparent chromatin bridging and a type 3b CEB showing symmetric and asymmetric mitosis. The last two images represent type 4 CEB aggregates revealing nucleus variations in size and maturation.

Table I - Patient findings

Patient type	Patient description	Type 1a	Type 1b	Type 1c	Type 1d	Type 2a	Type 2b	Type 3a	Type 3b	Type 4
1. Breast cancer, late stage	Treatment-naive recurrent breast cancer and bone, liver metastasis	3219	13	46	10	257	1	515	2	1260
2. Breast cancer, early stage	Postsurgery baseline, stage 2, lymph node negative	2	None	None	None	2	None	None	None	None
	Mid-term ACT	62	3	6	None	1	None	2	None	None
3. Small cell lung cancer, extensive stage	3 months 3rd regimen, brain metastasis	385	10	4	None	36	None	6	2	4
4. Lung adenocarcinoma, late stage	Treatment naive, stage 4	81	9	None	None	4	None	4	None	None
5. Head and neck, advanced stage	Under treatment	5	None	None	None	None	None	1	None	None
6. Diabetes	Healthy	6	None	None	None	1	None	1	None	None
7. Thrombocytosis	Stable thrombocytosis, healthy	2705	2	None	None	None	None	1	None	None
8. Osteoporosis	Osteoporosis healthy	9	None	1	None	1	None	None	None	None
9. Healthy	Data from Schreier et al. 2018 (n = 15)	7.5*	<1	None	None	None	None	None	None	None

ACT = adjuvant chemotherapy.
Numbers denote cell concentrations per 5mL whole blood.

so-called megaloblasts and macro-normoblasts, respectively. The finding of such abnormal morphologies in the circulation represents evidence of dyserythropoiesis and predicts a pathological state of the bone marrow (14,15). Megaloblasts show nucleocytoplasmic asynchrony and moderate to high and intracellular chromatin heterogeneity and high N/C ratio. Macro-normoblasts show no nucleocytoplasmic asynchrony, total condensation nuclei in a diameter of about 4 μm to 6 μm, and a very low N/C ratio. Type 2 CEB denotes an apparently relatively frequent morphological abnormality in both nonmalignant and malignant diseases and is characterized by symmetric multi-nucleation in a single cell most likely ascribed to asynchronous mitosis. Type 2 CEB may also vary in size and shape and includes aberrant cell types containing nuclei that differ in size and maturation (Fig. 1). We further divided type 2 CEB into binucleated (type 2a) and multinucleated or multinuclear lobulation single cells (type 2b) following World Health Organization (WHO) descriptions of bone marrow erythroblast abnormality (16). Different underlying pathologies and/or stages may be causative of the number of nuclei in a single cell, for example, in the classification of congenital dyserythropoietic anemia in which types I–IV directly correlate with the number of erythroblast nuclei (17). Myelodysplastic syndromes may produce three or more nucleated, yet mostly binucleated erythroblasts (15). Type 3 CEB denotes cells in synchronous mitosis at various stages from metaphase till cytokinesis and seems to occur across disease types as frequent as type 2a CEB. This type could be further divided into symmetric (type 3a) and aberrant (type 3b) cell morphologies. The latter includes CEB pairs showing internuclear bridging or containing nuclei that differ in size, number, and maturation (Fig. 1). Type 4 comprises cells appearing in groups of at least three round or oval, normal or binucleated cells and represents the morphological aspect of a cell cluster. These cells may be seen to be in division or constitute a breakaway of aggregated erythroblasts from an erythroid island within the bone marrow. Type 4 CEB is only found in late-stage malignancies.

Apart from types 1a and b, all other herein reported types were not found in the healthy cohort (8) (Tab. I). Therefore CEB types 1c, d, 2, 3, and 4 are herein referred to as abnormal and would denote bone marrow defects to some extent. According to Table I, the CEB profile with regard to heterogeneity and cell number may be positively correlated with disease severity, suggesting a relatively high sensitivity toward slightest physiological imbalances of the bone marrow.

Discussion

CRP is expected to convey a wealth of diagnostic information ascribed to lesion-associated cell egress into the blood stream or to tissue repair or maintenance. It is good to say that the rarest population of cells is most decisive for, and thus informative of, our health. Rare cells associated with tissue repair may comprise bone marrow-derived progenitor and stem cells. Those rare cells associated with lesions may comprise respective tissue-derived mature somatic cells, such as epithelial or endothelial cells. The diagnostic

exploitation of a single, a few, or all detectable circulating rare cells in a sample is referred to as cbLB. Our investigation in that field, in particular on the circulating CD71^{high} phenotype, has revealed a staggering variety of morphologies across different diseases that are seemingly not associated with pathological erythropoiesis and seem to correspond to findings of erythroid abnormality as could be found in the bone marrow (15). Erythrobast abnormality has been rarely reported to circulate, and to the best of our knowledge only in case of diseases with underlying pathological erythropoiesis (18). Apart from systemic diseases, treatment by chemotherapy is known to elevate CEB concentration (11), suggesting that CEB abnormality in patient 3 may be caused or influenced by chemotherapy. The two samples of patient 2 before and during chemoadjuvant therapy, respectively, would also support chemotherapy-induced CEB elevation.

We would like to take the opportunity to suggest possible clinical usefulness of our findings. The assumption is that CEB abnormality would denote sufficient cytological evidence to diagnose bone marrow defects and would allow us to grade BMD based on cell quantity and type. Cell aberration, in particular, and/or the finding of type 4 CEB could provide evidence for the association with more severe BMD as has been found exclusively in metastatic cancer (patients 1 and 3). Our thoughts about CEB abnormality and the association with BMD may be supported by investigations of the bone marrow pathology reporting similar erythroblast abnormality in case of severe bone marrow diseases, such as leukemia or hereditary anemia (18-20).

When applied to cancer, in particular early stage cancer patients may benefit from correct assessment of individualized distant invasion profiles (21) however, conventional functional imaging methods are not capable of detecting potentially hazardous distant micro-metastasis. Also, the detection of circulating tumor cells (CTCs) only predicts metastases based on statistics (22,23). Moreover, bone marrow biopsy may provide pathological evidence of distant disease development at the individual level, yet is not routinely performed given the patient risk by the procedure and low discrimination power between dormant and active invasion. Positive findings of tumor cell dissemination at earliest stages were commonly reported from bone marrow biopsies (24-26). Despite the evidence to support prognostic significance in early-stage breast cancer patients (27-30), bone marrow micro-metastases assessment (BMMA) as prognostic marker for relapse was found invariant to existing treatment decision making and, thus, was not adopted into clinical routine ever since (31). Henceforth, the diagnostic question of BMMA and single-cell invasion must be shifted from the status of distant invasion to distant aggressiveness, that is, BMD. The detection of CEB via cbLB could be a well-suited and better alternative to BMMA given the improved stratification power between dormant or inactive and active tumor cell invasion. We can expect from our data that dormant metastases would not produce marked CEB profiles and, vice versa, active disease would generate detectable CEB profiles. Finally, our BMD detection platform may tap into the exciting notion of CTC/DTC-guided treatment decision based on tumor evolution (32).

Conclusion

The study investigated circulating erythroid nucleated cells in the blood of healthy and afflicted individuals. Bone marrow-derived erythroblasts were identified in each blood donor by positive CD71 staining and typical erythroblast morphology confirming commonness as part of the blood rare cell population. Furthermore, abnormal erythroblast-like cells as known to the pathologist from bone marrow biopsies were found only in diseased individuals in this study. This report is mainly dedicated to the new finding of aberrant and mitotic erythroblast-like cells that are so far unknown to circulate in the blood of diseased individuals foremost in cancer patients. The cell abnormality could be coarsely classified into synchronous and asynchronous mitosis, respectively, and is likewise suspected to be bone marrow-derived, consequently indicating various degrees of BMD. A new cancer biomarker panel could be established in cbLB when used in combination with circulating epithelial cells as a potential detection and grading platform of cancer-associated active distant invasion.

Acknowledgments

We would like to give special thanks to Dr. Kanakorn Runglodvatana from Vajira Hospital, Bangkok, for providing head and neck cancer patient blood donation.

Ethics Approval and Consent to Participate

The study subject titled "Advancing cell-based liquid biopsy" was approved by the Mahidol University Central IRB, Mahidol University, with protocol number 2019/197.3007. All healthy donors were appointed, informed, and consented in written form. In case of the three cancer patient cases, study information was provided by the treating doctor and consent was given by the patient verbally, respectively during out patient consultation, due to very limited visitation time.

Abbreviations

ACT = adjuvant chemotherapy; BMD = bone marrow damage; BMMA = bone marrow micro-metastases assessment; cbLB = cell-based liquid biopsy; CEB = circulating erythroblast or circulating erythroblast-like cell; CTC = circulating tumor cell; DTC = disseminated tumor cells; H&N = head and neck cancer; N/C ratio: nucleus to cytoplasm ratio; RCP = rare cell population; SCLC = small cell lung cancer.

Disclosures

References

1. Millner LM, Linder MW, Valdes R Jr. Circulating tumor cells: a review of present methods and the need to identify heterogeneous phenotypes. Ann Clin Lab Sci. 2013;43(3):295-304. PubMed
2. Alix-Panabières C, Pantel K. Clinical applications of circulating tumor cells and circulating tumor DNA as liquid biopsy. Cancer Discov. 2016;6(5):479-491. CrossRef PubMed
3. Allard WJ, Matera J, Miller MC, et al. Tumor cells circulate in the peripheral blood of all major carcinomas but not in healthy subjects or patients with nonmalignant diseases. Clin Cancer Res. 2004;10(20):6897-6904. CrossRef PubMed
4. Bhakdi SC, Suriyaphol P, Thaicharoen P, et al. Accuracy of tumour-associated circulating endothelial cells as a screening biomarker for clinically significant prostate cancer. Cancers. 2019;11:1064. CrossRef PubMed
5. Jones ML, Siddiqui J, Pienta KJ, Getzenberg RH. Circulating fibroblast-like cells in men with metastatic prostate cancer. Prostate. 2013;73(2):176-181. CrossRef PubMed
6. Schreier S, Wannapong T. The blood circulating are cell population. What is it and what is it good for? Cells. 2020;9(4):790. CrossRef PubMed
7. Fadini GP, Avogaro A. It is all in the blood: the multifaceted contribution of circulating progenitor cells in diabetic complications. Exp Diabetes Res. 2012;2012:742976. CrossRef PubMed
8. Schreier S, Borwornpinyo S, Udomsangpetch R, Triampo W. An update of circulating rare cell types in healthy adult peripheral blood: findings of immature erythroid precursors. Ann Transl Med. 2018;6(20):406. CrossRef PubMed
9. Bessis M. L'ilot erythroblastique. Unite functionelle de la moelle osseuse. Rev Hematol (Paris). 1958;13:8-11.
10. Spike BT, Macleod KF. Effects of hypoxia on heterotypic macrophage interactions. Cell Cycle. 2007;6(21):2620-2624. CrossRef PubMed
11. Kobayashi Y, Takamatsu R, Sato S, et al. Erythroblast appearance associated with natalizumab. Mult Scler Relat Disord. 2019;29:145-147. CrossRef PubMed
12. Du R, Lu KV, Petritsch C, et al. HIF1a induces the recruitment of bone marrow-derived vascular modulatory cells to regulate tumor angiogenesis and invasion. Cancer Cell. 2008;13:206-220.
13. Sankaran VG, Orkin SH, Walkley CR. Rb intrinsically promotes erythropoiesis by coupling cell cycle exit with mitochondrial biogenesis. Genes Dev. 2008;22:463-475.
14. Downey H. The megaloblast-normoblast problem: a cytologic study. J Lab Clin Med. 1952;39(6):837-864. PubMed
15. Goasguen JE, Bennett JM, Bain BJ, et al; The International Working Group on Morphology of MDS. Dyserythropoiesis in the diagnosis of the myelodysplastic syndromes and other myeloid neoplasms: problem areas. Br J Haematol. 2018;182(4):526-533. CrossRef PubMed
16. Brunning RD, Orazi A, Germing U. Myelodysplastic syndromes/neoplasms, overview. In: World health organization classification of tumours of haematopoietic and lymphoid tissues 2008.
17. Iolascon A, Heimpel H, Wahlin A, Tamary H. Congenital dyserythropoietic anemias: molecular insights and diagnostic approach. Blood. 2013;122(13):2162-2166. CrossRef PubMed
18. Jaffray JA, Mitchell WB, Gnanapragasam MN, et al. Erythroid transcription factor EKLF/KLF1 mutation causing congenital dyserythropoietic anemia type IV in a patient of Taiwanese origin: review of all reported cases and development of a clinical diagnostic paradigm. Blood Cells Mol Dis. 2013;51(2):71-75. CrossRef PubMed
19. Zhao B, Liu H, Mei Y, et al. Disruption of erythroid nuclear opening and histone release in myelodysplastic syndromes. Cancer Med. 2019;8(3):1169-1174. CrossRef PubMed

20. Bright M, Cobb J, Evans B, Parry TE. Congenital dyserythropoietic anaemia with erythroblastic multinuclearity. J Clin Pathol. 1972;25(7):561-569. CrossRef PubMed

21. Pantel K, Cote RJ, Fodstad O. Detection and clinical importance of micrometastatic disease. J Natl Cancer Inst. 1999;91(13):1113-1124. CrossRef PubMed

22. Klein CA, Blankenstein TJ, Schmidt-Kittler O, et al. Genetic heterogeneity of single disseminated tumour cells in minimal residual cancer. Lancet. 2002;360(9334):683-689. CrossRef PubMed

23. Tharp D, Nandana S. How prostate cancer cells use strategy instead of brute force to achieve metastasis. *Cancers (Basel)*. 2019;11(12):1928. CrossRef PubMed

24. Diel IJ, Kaufmann M, Goerner R, Costa SD, Kaul S, Bastert G. Detection of tumor cells in bone marrow of patients with primary breast cancer: a prognostic factor for distant metastasis. J Clin Oncol. 1992;10(10):1534-1539. CrossRef PubMed

25. Walter VP, Taran FA, Wallwiener M, Brucker SY, Hartkopf AD . Abstract P1-01-16: Detection of disseminated tumor cells in DCIS patients impacts local recurrence. San Antonio Breast Cancer Symposium; December 5–9, 2017; San Antonio, Texas. Cancer Res. 2018. CrossRef

26. Banys M, Hahn M, Gruber I, et al. Detection and clinical relevance of hematogenous tumor cell dissemination in patients with ductal carcinoma in situ. Breast Cancer Res Treat. 2014;144(3):531-538. CrossRef PubMed

27. Cote RJ, Rosen PP, Lesser ML, Old LJ, Osborne MP. Prediction of early relapse in patients with operable breast cancer by detection of occult bone marrow micrometastases. J Clin Oncol. 1991;9(10):1749-1756. CrossRef PubMed

28. Mignot F, Loirat D, Dureau S, et al. Disseminated tumor cells predict efficacy of regional nodal irradiation in early stage breast cancer. Int J Radiat Oncol Biol Phys. 2019;103(2):389-396.

29. Braun S, Vogl FD, Naume B, et al. A pooled analysis of bone marrow micrometastasis in breast cancer. N Engl J Med. 2005;353(8):793-802. CrossRef PubMed

30. Stefanovic S, Diel I, Sinn P, et al. Disseminated tumor cells in the bone marrow of patients with operable primary breast cancer: prognostic impact in immunophenotypic subgroups and clinical implication for bisphosphonate treatment. Ann Surg Oncol. 2016;23(3):757-766. CrossRef PubMed

31. Harris L, Fritsche H, Mennel R, et al; American Society of Clinical Oncology. American Society of Clinical Oncology 2007 update of recommendations for the use of tumor markers in breast cancer. J Clin Oncol. 2007;25(33):5287-5312. CrossRef PubMed

32. Banys-Paluchowski M, Hartkopf A, Meier-Stiegen F, Janni W, Solomayer EF, Fehm T. Circulating and disseminated tumour cells in breast carcinoma: Report from the Consensus Conference on Tumour Cell Dissemination during the 38th Annual Meeting of the German Society of Senology, Berlin, 14 June 2018. Geburtshilfe Frauenheilkd. 2019;79(2):177-183. CrossRef PubMed

Serum IL-33 as a biomarker in different diseases: useful parameter or much need for clarification?

Stefan Erfurt[1], Meike Hoffmeister[2], Stefanie Oess[2], Katharina Asmus[1], Oliver Ritter[1], Susann Patschan[1], Daniel Patschan[1]

[1]Department of Medicine 1, University Hospital Brandenburg, Medical School (MHB) Theodor Fontane, Brandenburg - Germany
[2]Institute of Biochemistry, Brandenburg Medical School (MHB) Theodor Fontane, Brandenburg - Germany

ABSTRACT

Interleukin-33 (IL-33), a member of the IL-1 family, is critically involved in the modulation of the activity of a diverse range of immunocompetent cells. Essential roles have been implicated in cardioprotection, in both innate and adaptive immune responses in mucosal organs, and in the maintenance of adipose tissue cells. Over the past 10 years, several studies evaluated the usability of IL-33 as a biomarker in diseases of inflammatory and noninflammatory origin. Our group is currently evaluating the predictive role of serum IL-33 in acute kidney injury (AKI). The aim of the article is to discuss selected studies on IL-33 in different diseases and its potential role as a biomarker molecule.

Keywords: Biomarker, IL-33, Inflammatory diseases, Noninflammatory diseases

Introduction

The identification of biomarkers for either early diagnosis or risk prediction in various diseases remains a fundamental goal in the whole field of medicine. A sophisticated discussion of all or of at least the most important findings in recent years is impossible in one single article that is intended to focus on one potential marker molecule. The literature on biomarkers in even one particular disease, such as acute kidney injury (AKI), is vast. For illustrative purposes, it needs to be mentioned that more than 100 candidate molecules have been investigated in AKI subjects over the past 20 years (1). Only few parameters (e.g., NGAL, KIM-1 (2,3)) or combinations of two proteins such as the product of urinary insulin-like growth factor-binding protein (IGFBP-7) and tissue inhibitor of metalloproteinase (TIMP-2) (4,5) have been proven as reliable tools for diagnostic/prognostic purposes under certain AKI-associated conditions. However, no parameter can truly replace serum creatinine for measuring excretory kidney function in daily clinical practice, despite creatinine far from being an "optimal" biomarker. In 2019, our group

Corresponding author:
Daniel Patschan
Zentrum Innere Medizin 1
Universitätsklinikum Brandenburg
Medizinische Hochschule Brandenburg
Hochstraße 29
14770 Brandenburg - Germany
daniel.patschan@mhb-fontane.de

published a study on cytokine profiling in patients with ANCA-associated vasculitis (AAV) (6). Serum from healthy subjects and from patients with AAV or other autoimmune-mediated diseases was analyzed for concentrations of certain pro- and anti-inflammatory mediators. It became apparent that serum IL-33 was significantly higher in AAV subjects than in controls. Also, AAV patients with necrotizing glomerulonephritis (NGN) differed from AAV subjects without NGN. These findings led to the hypothesis of IL-33 as a potential biomarker in acute renal diseases, namely in AKI. The respective study has been initiated and is ongoing. The current article will summarize the most important references on IL-33 as a diagnostic tool and risk predictor in genetic and acquired diseases.

Interleukin-33—origin and physiology

Interleukin-33 (IL-33) belongs to the IL-1 family of cytokines (7). Common feature of the latter is a beta-trefoil structure, which has been identified in proteins such as IL-1alpha and -beta, IL-1Ra, and IL-18. IL-33 was initially found within endothelial cell nuclei of so-called human high endothelial venules (HEV). Baekkevold et al (8) described the protein as NF (nuclear factor)-HEV. Later, Pichery and colleagues (9) detected IL-33 within the nuclei of murine cells in various tissues, such as epithelial cells, lymphoid organs, brain, and embryonic tissue. Herein, the cytokine was expressed in a constitutive manner. In contrast, blood vessels did not show constitutive IL-33 expression. Within nuclei, IL-33 binds to chromatin (10); in the extracellular space however, it interacts with ST2. The latter exists as membrane-bound and soluble isoform (sST2), respectively (11). Interleukin-33 mediates so-called alarmin function. Alarmins, which are represented by extracellularly secreted proteins of various

origin and phenotype, indicate cell/tissue damage. Subsequently, immune cells are activated. In this context, IL-33 has been shown to modulate the activity of mast cells, group 2 innate lymphoid cells (ILC2s), T helper 2 cells, eosinophils, basophils, dendritic cells, macrophages, and others (12). Essential roles of the cytokine have been implicated in cardioprotection (11), in both innate and adaptive immune responses in mucosal organs (13) and in the maintenance of adipose tissue cells (via immune cell modulation) (14).

Quantification of serum IL-33

The data on IL-33 quantification by either ELISA (enzyme-linked immunosorbent assay) or multiplex technologies are heterogeneous. By far not all groups initially succeeded in measuring serum levels of the cytokine. Firstly, Krychtiuk and colleagues (15), who identified low serum IL-33 to be predictive in intensive care-treated patients, did not detect the protein in 57 out of 223 subjects. In 2016, Ketelaar et al (16) reported the results of serum IL-33 quantification by using four different ELISA kits (Quantikine and DuoSet, R&D systems, respectively; ADI-900-201, Enzo Life Sciences; SKR038, GenWay Biotech Inc, San Diego, USA). Serum samples were drawn from asthma patients. The authors included different numbers of samples per individual kit: Quantikine—n = 45; DuoSet—n = 17; ADI-900-201—n = 17; SKR038—n = 22. Surprisingly, the percentages of samples above the lower detection limit (LLD) were 0 (zero) in two kits (ADI-900-201 and SKR038). The Quantikine kit showed only 2% of all samples above the LLD, the DuoSet kit was successful in at least 76%. Comparable findings were reported by Asaka et al (17), who also employed the Quantikine kit. Difficulties in IL-33 quantification were also reported by Rivière and colleagues (18). In this context, it needs to be noted that erythrocytes contain IL-33 in relevant concentrations. Thus, hemolysis may increase serum IL-33 concentrations and potentially adulterate the findings in biomarker-related studies (19).

Aberrant IL-33 in diseases: elevation

Genetic disorders

Behairy and colleagues (20) evaluated 60 infants with cholestasis, assigned to one of two subgroups with versus without biliary atresia (BA and non-BA group). Subjects belonging to the first group showed significantly higher serum IL-33. Also, IL-33 was higher in both groups as compared to healthy controls. Finally, IL-33 correlated with aspartate and alanine aminotransferase (ALT), and with serum bilirubin in a positive manner, respectively. Since cytokine levels additionally correlated with the fibrosis stage, the authors concluded a potential (pathogenic) role of IL-33 in BA disease progression.

Cardiovascular diseases

A study in subjects with chronic kidney disease (CKD) was published in 2017 (21). Two-hundred and thirty-eight CKD patients were followed up for 24 months. Both serum

IL-33 and ST2, the circulating isoform of the IL-33 receptor, were quantified and associated with cardiovascular events and parameters of endothelial dysfunction (flow-mediated vasodilation, FMD). The two analytes increased with decreasing estimated glomerular filtration rate and elevated levels were associated with impaired FMD and cardiovascular risk. Nevertheless, Bao et al (22) failed to show increased IL-33 in CKD subjects. In experimental studies TGF-β KO (knock out) enhanced IL-33, and while its inflammatory regulation varies with the disease, in the heart it protects against pathological remodeling after infarction, myocyte hypoxia, pressure overload, and increased Ca^{2+} release from the SR (sarcoplasmic reticulum) which is tunneled to mitochondria via mitochondrial RyR, leading to stimulation of mitochondrial adenosine triphosphate production (23).

Autoimmune-mediated diseases

In 2010, Mu et al published data on rheumatoid arthritis (RA) (24). Three groups were evaluated: healthy controls, RA subjects, and patients with osteoarthritis. The cytokine was not detectable in controls and osteoarthritis but in almost 100 RA subjects (42.2%). Cytokine concentrations correlated with the RF and anti-CCP titers, respectively, and anti-TNF-alpha therapy reduced IL-33 serum levels. IL-33 elevation in RA was also shown by Hong and colleagues (25). Borsky et al (26) performed a study in psoriasis vulgaris subjects, intended to quantify serum levels of alarmins. The latter act as danger signals. The following factors were analyzed: HMGB1, IL-33, S100A7, and S100A12. In total, 63 psoriasis patients and 95 controls were included. All four proteins were elevated in a significant manner. Correlations between serum concentrations and disease activity were however not identified. Our group studied subjects with AAV and with other autoimmune-mediated diseases (6). Serum concentrations of the following parameters were measured: IL-1β, IL-6, IL-17 A, IL-17 F, IL-21, IL-22, IL-23, TNF-α, sCD40L, IL-4, IL-10, IL-25, IL-31, IL-33, and INF-γ. A total number of 62 AAV subjects were included in the study (39 females; 23 males). Forty-five subjects were PR3+, 17 subjects showed ANCA specificity for MPO (myeloperoxidase). Serum IL-33 was elevated in AAV and SSc (systemic sclerosis). In AAV, higher levels were found in non-NGN. Minaga et al (27) investigated a rarer type of disease, type 1 autoimmune pancreatitis (type 1 AIP), belonging to the heterogeneous group of IgG4-related disease (IgG4-RD). The study revealed higher levels of interferon-alpha and of IL-33 in type 1 AIP subjects in comparison to individuals with chronic pancreatitis of other origin and to healthy controls. Bakr et al (28) analyzed serum IL-33 in patients with pemphigus vulgaris. Affected subjects showed higher cytokine levels than healthy controls. Also, serum levels significantly correlated with the activity of the disease (measured by the Pemphigus Disease Area Index, PDAI).

Neoplasia

A study in patients with newly diagnosed prostate cancer was published in 2019 (29). One-hundred and fifty individuals were included. Serum IL-33 was higher than in controls,

particularly in subjects with higher disease stages. Nevertheless, cytokine concentrations did not differ between certain predefined genotypes. As a matter of fact, elevated IL-33 has also been documented in other malignant diseases such as gastric cancer (30), endometrial cancer (31), non-small cell lung cancer (32), and breast cancer (33).

Sepsis

Sepsis may be regarded as an archetype of a widespread inflammatory disease. In 2016, Çekmez and colleagues (34) reported data from 128 septic children (20 of these were controls). Finally, 68 individuals were excluded since blood cultures were negative. Serum IL-33 differed significantly between the two groups of controls vs sepsis (1.1 ± 0.28 ng/mL vs 5.23 ± 1.80 ng/mL; p = 0.01). Two years later, another study performed in septic children (neonates) (35) showed comparable findings with a rapid IL-33 increase at the first day after diagnosis, followed by a decrease over time (days 3 and 7).

Others

Although immune-mediated mechanisms are substantially involved in the pathogenesis of asthma bronchiale, the disorder has been placed in this section. Bahrami and colleagues (36) included 61 affected children and 63 healthy controls in their analyses and found serum IL-33 to be significantly elevated. Blood cytokine levels increased with increasing disease severity. The predictive value of serum IL-33 in polytraumatized subjects was analyzed by Halát and colleagues (37). The specific aim was to evaluate whether IL-33 is suitable for the prediction of pulmonary complications. The study included 130 patients, serum samples were obtained at the time of hospital admission and 2 days later. Subjects that developed both parenchymal lung injury and subsequent Acute Respiratory Distress Syndrome (ARDS) showed particularly high serum IL-33 at the time of admission. It was hypothesized that the cytokine is involved in promoting sustained lung injury in traumatized patients. Sundnes et al (38) also published a trial in traumatized individuals (n = 136). Plasma samples were collected at the time of hospital admission and several hours later (2, 4, 6, and 8 hours). The analyses showed a rapid and transient IL-33 increase in a subset of patients. The latter presented with more intense tissue injuries and a higher degree of coagulopathy. Another study related to serum patterns of alarmins (*Danger-Associated Molecular Patterns*—DAMPs) focused on schizophrenia. The following molecules were quantified: IL-33, sST2, HMGB1, and S100B (39). The study included 68 patients suffering from chronic schizophrenia and 29 healthy controls. All four analytes were higher in the disease group. It was concluded that alarmins may be involved in latent neuroinflammation underlying/perpetuating schizophrenia. Yuan and colleagues focused on chronic hepatitis B (CHB) (40). A total number of 130 CHB patients were included, 48 cases were defined as stable, 50 patients showed progression to acute-on-chronic liver failure (ACLF), 30 individuals also progressed but with overall milder dynamics (pre-ACLF). The highest IL-33 levels were detected in ACLF patients, associations were found with serum ALT, aspartate transaminase, and the Model End-Stage Liver Disease (MELD) score, respectively. The combination of serum IL-33 and the MELD score was predictive with regard to the 90-days mortality. Thus, IL-33 was proposed as prognostic marker in CHB-associated liver disease. In 2021, Venkataraman et al (41) published multiplex immune assay data from children with "Paediatric inflammatory multisystem syndrome temporally associated with SARS-CoV-2 infection (PIMS-TS)." Numerous cytokines were elevated, including IL-33. Duan and colleagues analyzed gout patients and found increased IL-33 in respective subjects with even higher levels in those individuals without impaired kidney function (42). Also, IL-33 was negatively correlated with markers of kidney dysfunction.

Aberrant IL-33 in diseases: suppression

Cardiovascular diseases

Experimental data showed neuroprotective effects of IL-33 (43,44). Therefore, Chen et al (45) evaluated the relationship between serum IL-33 and the risk for hemorrhage transformation (HT) of acute ischemic stroke (AIS) in humans. More than 150 individuals were included, none of these received thrombolytic therapy. Patients were assigned to the HT group if any radiographic signs of HT became apparent during the first 2 weeks after AIS diagnosis. Multivariate regression analysis identified IL-33 as an independent HT predictor (lower serum IL-33 levels were associated with higher HT risk). The authors expanded their analyses in the context of poststroke depression (46) and found a comparable (inverse) association between serum IL-33 and the risk for depression after AIS. Together, the data confirmed the concept of IL-33-mediated neuroprotection, even in humans. In this context, an important study by Li et al (47) evaluated long-term outcome variables of stroke patients in relation to initial serum IL-33. Higher cytokine levels were associated with a better 2-year outcome of affected individuals. Low serum IL-33 was finally also shown to be predictive in patients with intracerebral hemorrhage (48). A study in patients with heart failure with reduced ejection fraction (HF-REF) was published by Segiet et al (49). One hundred and fifty-five HF-REF individuals (males: 106, females: 49) were included, the mean left ventricular ejection fraction was 32.13 ±12.8%. Patients displayed lower mean serum IL-33 as compared to controls. Also, cytokine levels were lower in HF-REF of ischemic origin as opposed to HF-REF of other etiology.

Autoimmune-mediated diseases

A rarer autoimmune-mediated disorder (at least in central Europe), Behçet's disease was evaluated by Koca et al (50) who included 117 affected individuals. While patients' serum IL-33 did not differ from control levels, active disease states were associated with lower IL-33. Nevertheless, certain allelic variations did not differ in serum IL-33.

Others

In contrast to the study by Halát et al (37), who found IL-33 to be elevated in polytraumatized patients, another investigation performed in critically ill subjects showed opposite findings. Krychtiuk and colleagues (15) evaluated the predictive value of both IL-33 and sST2 with regard to the 30 days mortality in 223 intensive care patients. IL-33 was not detectable at all in 57 subjects. Serum IL-33 concentrations below the median strongly predicted death in an independent manner. Lower-than-normal IL-33 concentrations were also documented in osteoporosis (51) and in amyotrophic lateral sclerosis (52). Finally, Hasan et al (53) showed a negative correlation between IL-33 and the body mass index. They also found IL-33 to negatively correlate with HbA1C in non-diabetic individuals.

No aberrant IL-33 in diseases

Cardiovascular diseases

Firouzabadi and colleagues (54) measured serum IL-33 and the soluble isoform of its receptor (sST2) in 44 heart failure patients (n = 25 under carvedilol treatment vs n = 19 without beta-blocker therapy) and in 22 healthy controls. The analyses did not reveal any differences between any of the three groups, which led to the conclusion that cardio-protective effects of carvedilol are most likely not mediated via the IL-33/sSTs axis. Two other studies related to acute cardiovascular diseases did also not show any differences in serum IL-33 between controls and patients. Demyanets et al (55) investigated subjects with stable angina, NSTEMI (non-ST-segment elevation myocardial infarction), or STEMI in comparison to healthy controls. Dhillon and colleagues (56) analyzed NSTEMI subjects.

Table I summarizes studies on serum IL-33 in diseases, assigned to one out of three groups: elevation/suppression or constant IL-33.

Conclusions

The data on serum IL-33 in human diseases are heterogeneous. On the one hand, methodological difficulties in measuring serum IL-33 may occur and must always be put into consideration if low levels or no protein at all is detectable. The majority of studies in which IL-33 quantification

TABLE I - Studies in serum IL-33 in inflammatory and noninflammatory disorders

IL-33 elevation	IL-33 suppression	Constant IL-33
Biliary atresia (20)	HT of AIS (45)	Heart failure (54)
CKD (21)	Poststroke depression (46)	CKD (22)
Rheumatoid arthritis (24)	Long-term outcome after stroke (47)	Stable angina pectoris, NSTEMI, STEMI (55)
Rheumatoid arthritis (25)	Intracerebral hemorrhage (48)	NSTEMI (56)
Psoriasis vulgaris (26)	HF-REF (49)	
Prostate cancer (29)	Behçet's disease (50)	
Gastric cancer (30)	Critically ill subjects (15)	
Endometrial cancer (31)	Osteoporosis (51)	
Non–small cell lung cancer (32)	Amyotrophic lateral sclerosis (52)	
Breast cancer (33)	Increased body weight (53)	
Sepsis in infants (34)		
Sepsis in infants (35)		
Asthma bronchiale in children (36)		
Polytrauma (37)		
Trauma (38)		
ANCA-associated vasculitis (6)		
Pemphigus vulgaris (28)		
Type 1 autoimmune pancreatitis (27)		
Schizophrenia (39)		
Hepatitis B-associated acute-on-chronic liver failure (40)		
PIMS-TS (41)		
gout (42)		

References appear according to the order in the text.
AIS = acute ischemic stroke; CKD = chronic kidney disease; HF-REF = heart failure with reduced ejection fraction; HT = hemorrhage transformation; IL = interleukin; NSTEMI = non-ST-segment elevation myocardial infarction; PIMS-TS = pediatric inflammatory multisystem syndrome temporally associated with SARS-CoV-2 infection.

succeeded showed higher blood concentrations of the cytokine. However, to identify a pattern that potentially allowed conclusions on the exact role of serum IL-33 in inflammatory and noninflammatory diseases is quite difficult. We cited a total number of 21 studies that reported IL-33 elevation under pathological circumstances. Thirteen out of these 21 investigations evaluated diseases with distinct inflammatory pathogenesis (exceptions: CKD, BA, schizophrenia, five malignancies). Two out of 10 studies reporting lower IL-33 were nevertheless also performed in inflammatory disease states (Behçet's disease, critically ill subjects). Thus, it may be concluded that elevation of serum IL-33 should be expected with higher probability in inflammatory than in noninflammatory disorders. The references on malignancies with elevated IL-33 were all referring to carcinomas. Activation of the immune system is known to significantly occur in malignant disorders. It is therefore not surprising that diseases such as heart failure with preserved or reduced ejection fraction, ischemic stroke, or even most cases of AKI are not associated with increased serum IL-33. Regarding the heterogeneity of diseases with either IL-33 elevation or suppression, it is hardly possible to propose the molecule as *specific* biomarker at the moment.

Disclosures

References

1. Schrezenmeier EV, Barasch J, Budde K, Westhoff T, Schmidt-Ott KM. Biomarkers in acute kidney injury—pathophysiological basis and clinical performance. Acta Physiologica (Oxford, England). 2016.

2. Huo W, Zhang K, Nie Z, Li Q, Jin F. Kidney injury molecule-1 (KIM-1): a novel kidney-specific injury molecule playing potential double-edged functions in kidney injury. Transplant Rev (Orlando). 2010;24(3):143-146. CrossRef PubMed

3. Shang W, Wang Z. The update of NGAL in acute kidney injury. Curr Protein Pept Sci. 2017;18(12):1211-1217. CrossRef PubMed

4. Fan W, Ankawi G, Zhang J, et al. Current understanding and future directions in the application of TIMP-2 and IGFBP7 in AKI clinical practice. Clin Chem Lab Med. 2019;57(5):567-576. CrossRef PubMed

5. Nalesso F, Cattarin L, Gobbi L, Fragasso A, Garzotto F, Calò LA. Evaluating Nephrocheck® as a predictive tool for acute kidney injury. Int J Nephrol Renovasc Dis. 2020;13:85-96. CrossRef PubMed

6. Hoffmann JC, Patschan D, Dihazi H, et al. Cytokine profiling in anti neutrophil cytoplasmic antibody-associated vasculitis: a cross-sectional cohort study. Rheumatol Int. 2019;39(11): 1907-1917. CrossRef PubMed

7. Fields JK, Günther S, Sundberg EJ. Structural basis of IL-1 family cytokine signaling. Front Immunol. 2019;10:1412. CrossRef PubMed

8. Baekkevold ES, Roussigné M, Yamanaka T, et al. Molecular characterization of NF-HEV, a nuclear factor preferentially expressed in human high endothelial venules. Am J Pathol. 2003;163(1):69-79. CrossRef PubMed

9. Pichery M, Mirey E, Mercier P, et al. Endogenous IL-33 is highly expressed in mouse epithelial barrier tissues, lymphoid organs, brain, embryos, and inflamed tissues: in situ analysis using a novel Il-33-LacZ gene trap reporter strain. J Immunol. 2012;188(7):3488-95.

10. Roussel L, Erard M, Cayrol C, Girard JP. Molecular mimicry between IL-33 and KSHV for attachment to chromatin through the H2A-H2B acidic pocket. EMBO Rep. 2008;9(10):1006-1012. CrossRef PubMed

11. Kotsiou OS, Gourgoulianis KI, Zarogiannis SG. IL-33/ST2 axis in organ fibrosis. Front Immunol. 2018;9:2432. CrossRef PubMed

12. Cayrol C, Girard JP. Interleukin-33 (IL-33): a nuclear cytokine from the IL-1 family. Immunol Rev. 2018;281(1):154-168. CrossRef PubMed

13. Drake LY, Kita H. IL-33: biological properties, functions, and roles in airway disease. Immunol Rev. 2017;278(1):173-184. CrossRef PubMed

14. de Oliveira MFA, Talvani A, Rocha-Vieira E. IL-33 in obesity: where do we go from here? Inflamm Res. 2019;68(3):185-194. CrossRef PubMed

15. Krychtiuk KA, Stojkovic S, Lenz M, et al. Predictive value of low interleukin-33 in critically ill patients. Cytokine. 2018;103: 109-113. CrossRef PubMed

16. Ketelaar ME, Nawijn MC, Shaw DE, Koppelman GH, Sayers I. The challenge of measuring IL-33 in serum using commercial ELISA: lessons from asthma. Clin Exp Allergy. 2016;46(6): 884-887. CrossRef PubMed

17. Asaka D, Yoshikawa M, Nakayama T, Yoshimura T, Moriyama H, Otori N. Elevated levels of interleukin-33 in the nasal secretions of patients with allergic rhinitis. Int Arch Allergy Immunol. 2012;158(s1)(suppl 1):47-50. CrossRef PubMed

18. Rivière E, Ly B, Boudaoud S, et al. Pitfalls for detecting interleukin-33 by ELISA in the serum of patients with primary Sjögren syndrome: comparison of different kits. Ann Rheum Dis. 2016;75(3):633-635. CrossRef PubMed

19. Wei J, Zhao J, Schrott V, et al. Red blood cells store and release interleukin-33. J Investig Med. 2015;63(6):806-810. CrossRef PubMed

20. Behairy OG, Elsadek AE, Behiry EG, Elhenawy IA, Shalan NH, Sayied KR. Clinical value of serum interleukin-33 biomarker in infants with neonatal cholestasis. J Pediatr Gastroenterol Nutr. 2020;70(3):344-349. CrossRef PubMed

21. Gungor O, Unal HU, Guclu A, et al. IL-33 and ST2 levels in chronic kidney disease: associations with inflammation, vascular abnormalities, cardiovascular events, and survival. PLoS One. 2017;12(6):e0178939. CrossRef PubMed

22. Bao YS, Na SP, Zhang P, et al. Characterization of interleukin-33 and soluble ST2 in serum and their association with disease severity in patients with chronic kidney disease. J Clin Immunol. 2012;32(3):587-594. CrossRef PubMed

23. Seidlmayer LK, Kuhn J, Berbner A, et al. Inositol 1,4,5-trisphosphate-mediated sarcoplasmic reticulum-mitochondrial crosstalk influences adenosine triphosphate production via mitochondrial Ca2+ uptake through the mitochondrial ryanodine receptor in cardiac myocytes. Cardiovasc Res. 2016;112(1): 491-501. CrossRef PubMed

24. Mu R, Huang HQ, Li YH, Li C, Ye H, Li ZG. Elevated serum interleukin 33 is associated with autoantibody production in

patients with rheumatoid arthritis. J Rheumatol. 2010;37(10): 2006-2013. CrossRef PubMed

25. Hong YS, Moon SJ, Joo YB, et al. Measurement of interleukin-33 (IL-33) and IL-33 receptors (sST2 and ST2L) in patients with rheumatoid arthritis. J Korean Med Sci. 2011;26(9): 1132-1139. CrossRef PubMed

26. Borsky P, Fiala Z, Andrys C, et al. Alarmins HMGB1, IL-33, S100A7, and S100A12 in psoriasis vulgaris. Mediators Inflamm. 2020;2020:8465083. CrossRef PubMed

27. Minaga K, Watanabe T, Hara A, et al. Identification of serum IFN-α and IL-33 as novel biomarkers for type 1 autoimmune pancreatitis and IgG4-related disease. Sci Rep. 2020;10(1):14879. CrossRef PubMed

28. Bakr RM, Sayed DS, Abd-Elkader AS, Kamel AA, Badran AY. Does interleukin-33 level correlate with the activity of pemphigus vulgaris?: A case-control study. Dermatol Ther. 2021;34(1): e14605. CrossRef PubMed

29. Chatrabnous N, Jafarzadeh A, Ghaderi A, et al. Association of elevated interleukin-33 serum levels with tumor stages in patients with prostate cancer. Eur Cytokine Netw. 2019;30(4): 144-150. PubMed

30. Sun P, Ben Q, Tu S, Dong W, Qi X, Wu Y. Serum interleukin-33 levels in patients with gastric cancer. Dig Dis Sci. 2011;56 (12):3596-3601. CrossRef PubMed

31. Zeng X, Zhang Z, Gao QQ, et al. Clinical significance of serum interleukin-31 and interleukin-33 levels in patients of endometrial cancer: a case control study. Dis Markers. 2016;2016: 9262919. CrossRef PubMed

32. Hu LA, Fu Y, Zhang DN, Zhang J. Serum IL-33 as a diagnostic and prognostic marker in non-small cell lung cancer. Asian Pac J Cancer Prev. 2013;14(4):2563-2566. CrossRef PubMed

33. Yang ZP, Ling DY, Xie YH, et al. The association of serum IL-33 and sST2 with breast cancer. Dis Markers. 2015;2015:516895. CrossRef PubMed

34. Çekmez F, Fidanci MK, Ayar G, et al. Diagnostic value of Upar, IL-33, and ST2 levels in childhood sepsis. Clin Lab. 2016;62(5): 751-755. CrossRef PubMed

35. Halil H, Tayman C, Buyuktiryaki M, Okur N, Cakır U, Serkant U. Serum interleukin-33 as a biomarker in predicting neonatal sepsis in premature infants. Comb Chem High Throughput Screen. 2018;21(7):510-515. CrossRef PubMed

36. Bahrami Mahneh S, Movahedi M, Aryan Z, et al; Universal Scientific Education and Research Network (USERN). Serum IL-33 is elevated in children with asthma and is associated with disease severity. Int Arch Allergy Immunol. 2015;168(3):193-196. CrossRef PubMed

37. Halát G, Haider T, Dedeyan M, Heinz T, Hajdu S, Negrin LL. IL-33 and its increased serum levels as an alarmin for imminent pulmonary complications in polytraumatized patients. World J Emerg Surg. 2019;14(1):36. CrossRef PubMed

38. Sundnes O, Ottestad W, Schjalm C, et al. Rapid systemic surge of IL-33 after severe human trauma: a prospective observational study. Mol Med. 2021;27(1):29. CrossRef PubMed

39. Kozłowska E, Brzezińska-Błaszczyk E, Agier J, Wysokiński A, Żelechowska P. Alarmins (IL-33, sST2, HMGB1, and S100B) as potential biomarkers for schizophrenia. J Psychiatr Res. 2021; 138:380-387. CrossRef PubMed

40. Yuan W, Mei X, Zhang YY, et al. High expression of interleukin-33/ST2 predicts the progression and poor prognosis in

chronic hepatitis B patients with hepatic flare. Am J Med Sci. 2020;360(6):656-661. CrossRef PubMed

41. Venkataraman A, Kumar NP, Hanna LE, et al. Plasma biomarker profiling of PIMS-TS, COVID-19 and SARS-CoV2 seropositive children—a cross-sectional observational study from southern India. EBioMedicine. 2021;66:103317. CrossRef PubMed

42. Duan L, Huang Y, Su Q, et al. Potential of IL-33 for preventing the kidney injury via regulating the lipid metabolism in gout patients. J Diabetes Res. 2016;2016:1028401. CrossRef PubMed

43. Jiao M, Li X, Chen L, et al. Neuroprotective effect of astrocyte-derived IL-33 in neonatal hypoxic-ischemic brain injury. J Neuroinflammation. 2020;17(1):251. CrossRef PubMed

44. Liu X, Hu R, Pei L, et al. Regulatory T cell is critical for interleukin-33-mediated neuroprotection against stroke. Exp Neurol. 2020;328:113233. CrossRef PubMed

45. Chen Z, Hu Q, Huo Y, Zhang R, Fu Q, Qin X. Serum interleukin-33 is a novel predictive biomarker of hemorrhage transformation and outcome in acute ischemic stroke. J Stroke Cerebrovasc Dis. 2021;30(2):105506. CrossRef PubMed

46. Chen Z, Zhang R, Wu Y, Fu Q, Qin X. Serum interleukin-33 is a predictor of depression in patients with acute ischemic stroke. Curr Neurovasc Res. 2020;17(5):719-724. CrossRef PubMed

47. Li XM, Wang XY, Feng XW, et al. Serum interleukin-33 as a novel marker for long-term prognosis and recurrence in acute ischemic stroke patients. Brain Behav. 2019;9(9):e01369. CrossRef PubMed

48. Miao Y, Zhang ZX, Feng X, Sun WM. IL-33 as a novel serum prognostic marker of intracerebral hemorrhage. Oxid Med Cell Longev. 2021;2021:5597790. CrossRef PubMed

49. Segiet OA, Romuk E, Nowalany-Kozielska E, Wojciechowska C, Piecuch A, Wojnicz R. The concentration of interleukin-33 in heart failure with reduced ejection fraction. Anatol J Cardiol. 2019;21(6):305-313. CrossRef PubMed

50. Koca SS, Kara M, Deniz F, et al. Serum IL-33 level and IL-33 gene polymorphisms in Behçet's disease. Rheumatol Int. 2015;35(3):471-477. CrossRef PubMed

51. Ginaldi L, De Martinis M, Saitta S, et al. Interleukin-33 serum levels in postmenopausal women with osteoporosis. Sci Rep. 2019;9(1):3786. CrossRef PubMed

52. Lin CY, Pfluger CM, Henderson RD, McCombe PA. Reduced levels of interleukin 33 and increased levels of soluble ST2 in subjects with amyotrophic lateral sclerosis. J Neuroimmunol. 2012;249(1-2):93-95. CrossRef PubMed

53. Hasan A, Al-Ghimlas F, Warsame S, et al. IL-33 is negatively associated with the BMI and confers a protective lipid/metabolic profile in non-diabetic but not diabetic subjects. BMC Immunol. 2014;15(1):19. CrossRef PubMed

54. Firouzabadi N, Dashti M, Dehshahri A, Bahramali E. Biomarkers of IL-33 and sST2 and lack of association with carvedilol therapy in heart failure. Clin Pharmacol. 2020;12:53-58. CrossRef PubMed

55. Demyanets S, Speidl WS, Tentzeris I, et al. Soluble ST2 and interleukin-33 levels in coronary artery disease: relation to disease activity and adverse outcome. PLoS One. 2014;9(4):e95055. CrossRef PubMed

56. Dhillon OS, Narayan HK, Quinn PA, Squire IB, Davies JE, Ng LL. Interleukin 33 and ST2 in non-ST-elevation myocardial infarction: comparison with Global Registry of Acute Coronary Events Risk Scoring and NT-proBNP. Am Heart J. 2011;161(6):1163-1170. CrossRef PubMed

Open Access

Pharmacokinetics of the disialoganglioside, G_{D2}, a circulating tumor biomarker for neuroblastoma, in nonhuman primates

Frank M. Balis[1], Cynthia Lester McCully[2], Christine M. Busch[1], Elizabeth Fox[3], Katherine E. Warren[2]

[1]Children's Hospital of Philadelphia, Philadelphia, PA - USA
[2]Pediatric Oncology Branch, National Cancer Institute, NIH, Bethesda, MD - USA
[3]St. Jude Children's Research Hospital, Memphis, TN - USA

ABSTRACT

Background: The ganglioside G_{D2} is a potential circulating tumor biomarker for the childhood cancer neuroblastoma. Interpreting the levels of a circulating tumor biomarker depends in part on a knowledge of the biomarker's clinical pharmacology.
Methods: We studied the plasma and cerebrospinal fluid (CSF) pharmacokinetics of the C_{18} lipoform of G_{D2} in two nonhuman primates with indwelling subcutaneous CSF lateral ventricular reservoir systems. G_{D2} was quantified with a validated high-performance liquid chromatography (HPLC)/tandem mass spectrometry assay. G_{D2} was administered as a short intravenous infusion and frequent plasma and CSF samples were drawn over 72 hours.
Results: G_{D2} plasma concentration declined monoexponentially with a half-life of 16 hours. Clearance was 0.0136 and 0.0131 L/h and volume of distribution (V_d) was 0.035 and 0.038 L/kg in the two animals. V_d was equivalent to plasma volume. Greater than 98% of G_{D2} in plasma is in a bound form consistent with its known association with lipoproteins and accounting for its limited volume of distribution. G_{D2} did not cross over from plasma into the CSF.
Conclusions: The pharmacokinetic profile of G_{D2} is favorable for a circulating tumor biomarker. This study demonstrates the value of characterizing the clinical pharmacology of circulating biomarkers to better understand their clinical behavior.

Keywords: Biomarker, Ganglioside, Neuroblastoma, Pharmacokinetics

Introduction

The ganglioside G_{D2} is a constituent of the plasma membrane of neuronal cells and is also expressed on the surface of the childhood cancer, neuroblastoma, and other cancers of neuroectodermal origin, such as melanoma. G_{D2} has a lipid domain (ceramide) that inserts into the plasma membrane and a 5-membered glycan domain that contributes to the glycocalyx on the cell surface. The glycan domain contains 2 sialic acid groups that are fully ionized in the physiological pH range.

G_{D2} circulates in low nanomolar concentrations in children, but its concentration is 30-fold elevated compared to controls in the serum of children with high-risk/high-stage neuroblastoma (1). We developed and validated a sensitive and specific high-performance liquid chromatography (HPLC)/tandem mass spectrometry assay to quantify the circulating lipoforms of G_{D2}, and we are evaluating G_{D2} as a circulating tumor biomarker for neuroblastoma. The C_{18} lipoform (18-carbon fatty acid chain length in ceramide) is the predominant form of G_{D2} in the plasma of patients with neuroblastoma.

Interpreting the results of a circulating tumor biomarker depends in part on a knowledge of the biomarker's clinical pharmacology. The steady-state circulating concentration of a tumor biomarker is determined by its rate of production by the tumor and by its clearance. Slow clearance results in accumulation of the biomarker in the plasma and enhances the sensitivity for detecting low tumor burden. However, a slowly cleared biomarker is not responsive to rapid changes in tumor burden (e.g., surgical resection). For example, an α-fetoprotein (AFP) concentration exceeding 100,000 ng/mL can take more than 2 months to fall into the reference range after complete resection of an AFP-producing tumor. Conversely, a rapidly eliminated tumor biomarker will not accumulate in the circulation, but its concentration may better reflect changes in tumor burden in real time.

We studied the pharmacokinetics and cerebrospinal fluid (CSF) penetration of G_{D2} after intravenous administration of the ganglioside to two nonhuman primates (NHPs) with indwelling subcutaneous CSF lateral ventricular reservoirs that allow for rapid, serial CSF sampling (2).

Methods

Chemicals

Purified human brain-derived G_{D2} was purchased from EMD Millipore Corp. (Billerica, MA) and contains two dominant lipoforms of G_{D2}—D18: 1-18:0 (C_{18}, molecular weight 1674.9 g/mol) and D18: 1-20:0 (C_{20}). G_{D2} was dissolved in a small volume of dimethyl sulfoxide (DMSO), diluted in sterile normal saline, and filter sterilized through a 22-micron filter. A sample of the filtered drug solution was assayed for content of the C_{18} lipoform of G_{D2} to quantify the administered dose.

Animals

This study was approved by the National Cancer Institute Animal Care and Use Committee. Two adult male rhesus monkeys (*Macaca mulatta*), weighing 8.0 and 8.6 kg, respectively, were humanely utilized for this study and were cared for in accordance with the National Research Council Guide for the Care and Use of Laboratory Animals, 8th edition (3). Animals were socially housed when possible. Both subjects had previously undergone implantation of an indwelling lateral ventricular catheter, which was attached to a subcutaneously implanted CSF reservoir (2). The subjects also had subcutaneously implanted femoral venous access ports for sampling blood. Each subject had a veterinary physical and neurological examination and blood chemistries and complete blood counts performed prior to G_{D2} administration to ensure they were physiologically and neurologically within normal limits. After G_{D2} administration the subjects were observed for adverse events daily for 2 weeks and had biweekly clinical chemistries and complete blood counts.

G_{D2} was administered as a 10-minute intravenous infusion through a temporary catheter in the cephalic or saphenous vein. Blood was serially sampled from the femoral venous access port and CSF was sampled from the subcutaneous CSF reservoir.

Sample times and sample processing

Blood (3 mL) and CSF (0.3 mL) were collected prior to the G_{D2} infusion, at the end of the 10-minute infusion, and 0.25, 1, 2, 4, 6, 8, 24, 48, and 72 hours postinfusion. Blood was collected in heparinized tubes and placed on ice. Plasma was separated by centrifugation at 4°C. Plasma and CSF were stored frozen at −80°C until assayed.

Sample analysis

The concentration of the C_{18} lipoform of G_{D2} in plasma and CSF samples was quantified using a previously reported, validated HPLC/tandem mass spectrometry method with a lower limit of quantification of 3 nM (4). Human brain-derived G_{D2},

which is made up of approximately 60% C_{20} and 40% C_{18} lipoforms, was used to construct the standard curves for the assay.

Pharmacokinetic analysis

A one-compartment pharmacokinetic model with first-order elimination was individually fit to the plasma concentration-time data from the 2 subjects using Phoenix NLME v.8.3 (Certara, Princeton, NJ). Model parameters are clearance (CL) and volume of distribution (V_d). The elimination rate constant (k_{el}) was derived from CL/V_d, the half-life from $0.693/k_{el}$, the area under the concentration-time curve (AUC) from dose/CL, and the mean residence time (MRT) from $1/k_{el}$.

Protein binding

Human plasma was spiked with human brain-derived G_{D2} to achieve a 200 nM concentration of the C_{18} lipoform. Spiked plasma was centrifuged through a Vivaspin 500 concentrator with a 300,000 molecular weight cutoff (MWCO) polyethersulfone (PES) membrane (Sartorius, Goettingen, Germany). G_{D2} concentration was measured in the concentrate that remained above the PES membrane and the effluent that passed through the PES membrane.

Results

The predose concentrations of C_{18} G_{D2} in the 2 subjects were 5.0 and 3.7 nM in plasma and 4.0 and 8.9 nM in CSF. The predose plasma concentrations in the subjects are similar to G_{D2} concentrations in control human plasma (1). End-of-infusion G_{D2} plasma concentrations were 1,390 and 1,090 nM, and concentrations declined in the plasma in a monoexponential fashion (Fig. 1). Pharmacokinetic parameters for
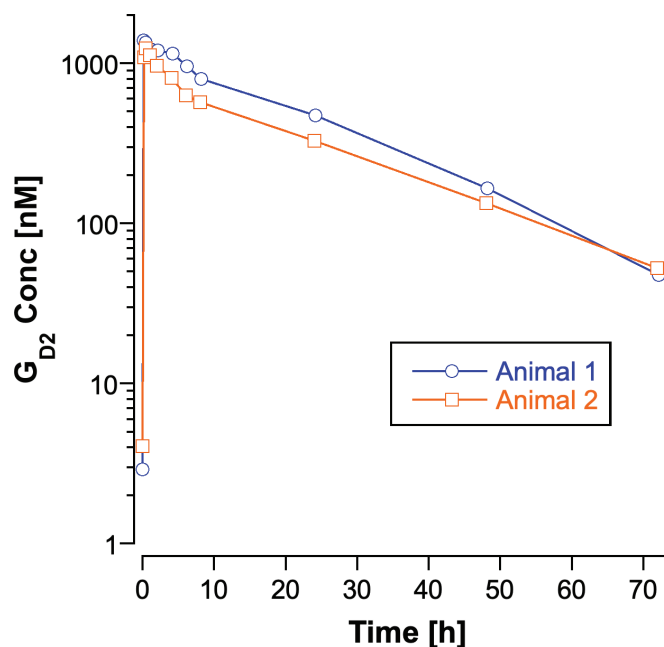
Fig. 1 - Plasma concentration-time curve for the C_{18} lipoform of G_{D2} in 2 nonhuman primates after a short intravenous infusion.

Animal	Weight (kg)	Dose (nmol)	Volume of Distribution (L/kg)	Clearance (L/h)	k$_{el}$ (h^{-1})	AUC (nM · h)	Half-life (h)	MRT (h)
1 (ZB39)	8.6	402	0.0354	0.0136	0.0448	29,500	15.5	22.3
2 (ZJ57)	8.0	313	0.0384	0.0131	0.0427	23,800	16.2	23.4

k$_{el}$ = first-order elimination rate constant; AUC = area under the concentration-time curve; MRT = mean residence time.

C$_{18}$ G$_{D2}$ for the 2 subjects are listed in Table I. The administered dose of G$_{D2}$ was estimated from the volume of drug solution administered and the concentration of C$_{18}$ G$_{D2}$ in the postfiltration drug solution. Intersubject variability in the pharmacokinetic parameters was minimal. The volume of distribution of G$_{D2}$ approximated plasma volume (blood volume in adult rhesus macaques is 0.062 L/kg (5)). Clearance of G$_{D2}$ from the circulation was slow with a half-life of 16 hours.

C$_{18}$ G$_{D2}$ concentrations remained at or near baseline levels in CSF throughout the 72-hour sampling period. The peak CSF concentration in animal 1 was 9.0 nM at the end of the infusion (baseline concentration was 4.0 nM), and CSF concentrations in animal 2 did not exceed the baseline concentration of 8.9 nM.

More than 98% of C$_{18}$ G$_{D2}$ in human plasma (200 nM) was retained in the plasma concentrate (above the membrane) after centrifugation through the Vivaspin 500 concentrator with a 300,000 MWCO PES membrane. The effluent G$_{D2}$ concentration was 4.5 nM after 15 minutes of centrifugation.

Conclusions

The disialoganglioside G$_{D2}$ is expressed in the cell membrane of neuroblastoma tumor cells and is shed into the circulation in patients with high-risk/high-stage disease (1,6). Prospective studies are ongoing to assess its potential utility as a circulating tumor biomarker for high-risk neuroblastoma. We characterized the pharmacokinetics of G$_{D2}$ in a NHP CSF access model that has proven to be predictive of human plasma and CSF disposition for a wide variety of drugs (7) in order to better understand the clinical behavior of circulating G$_{D2}$. The pharmacokinetic parameters from this study should prove useful for interpreting serial G$_{D2}$ concentrations monitored over the course of a patient's disease.

The pharmacokinetic characteristics of G$_{D2}$ are favorable for a circulating tumor biomarker. The 16 hours half-life in plasma indicates that G$_{D2}$ should be rapidly responsive to changes in tumor burden. After treatment, a new steady-state concentration should be reached within 3 to 4 days (5 half-lives), suggesting that plasma G$_{D2}$ concentration could be useful for assessing treatment effect in near real time. The limited volume of distribution, which is equivalent to plasma volume in NHPs, enhances sensitivity because the G$_{D2}$ is concentrated in (limited to) the compartment from which it is being measured. If G$_{D2}$ were more widely distributed throughout the body, the concentration in plasma would be proportionally lower.

Ultrafiltration of plasma spiked with G$_{D2}$ showed that it circulates in a bound form with a large molecular weight. This is consistent with the previously reported association of G$_{D2}$ and other gangliosides with lipoproteins, which have molecular weights in excess of 3,000 kDa (8). G$_{D2}$ is not detectable in lipoprotein-depleted plasma and is primarily associated with low-density lipoproteins (LDLs) (8). Binding of G$_{D2}$ to LDL and, to a lesser extent, other lipoproteins accounts for the volume of distribution being limited to plasma volume, and likely also accounts for the lack of G$_{D2}$ penetration into the CSF in the NHP CSF access model. Detecting G$_{D2}$ in the CSF of patients with neuroblastoma could be an indicator of brain or meningeal tumor spread even in the presence of high plasma G$_{D2}$ concentrations.

The anti-G$_{D2}$ monoclonal antibody, dinutuximab, is a component of the frontline treatment of neuroblastoma. Circulating G$_{D2}$ could theoretically bind to dinutuximab and block the binding of the antibody to G$_{D2}$ on the surface of tumor cells. Dinutuximab binds to the glycan portion of G$_{D2}$ that resides on the cell surface. The configuration of G$_{D2}$ in LDL is likely to be similar to that in the cell membrane with the polar glycan portion on the surface of the lipoprotein complex and the ceramide portion extending into the nonpolar core. Therefore, even though G$_{D2}$ is essentially all bound to lipoproteins in the circulation, the antigenic glycan portion may still be exposed on the surface for binding to dinutuximab.

Dinutuximab immunotherapy is currently administered in the final phase of neuroblastoma therapy, when plasma G$_{D2}$ concentrations are likely to be low, but pilot studies are ongoing to investigate the use of dinutuximab in the initial phase of therapy when circulating G$_{D2}$ concentrations are likely to be higher in some patients. Binding of the antibody to lipoprotein-associated G$_{D2}$ could lower the efficacy of dinutuximab by limiting the amount of antibody available to bind to tumor cells.

The pharmacokinetic profile of G$_{D2}$ is favorable for a circulating tumor biomarker. With its relatively short half-life, plasma G$_{D2}$ concentrations should reflect changes in tumor burden with a minimal lag time, and the limited volume of distribution translates into higher concentrations in plasma, improving its sensitivity. This study demonstrates the value of characterizing the clinical pharmacology of circulating biomarkers to better understand their clinical behavior. The use of the NHP model that is predictive of human pharmacokinetics provided the opportunity to study the pharmacokinetics of G$_{D2}$ after administration of a known dose and without interference from endogenous production. We plan to confirm the results using a more limited sampling approach in children with neuroblastoma after definitive treatment.

Disclosures

References

1. Balis FM, Busch CM, Desai AV, et al. The ganglioside G_{D2} as a circulating tumor biomarker for neuroblastoma. Pediatr Blood Cancer. 2020;67(1):e28031. CrossRef PubMed
2. Lester McCully CM, Bacher J, MacAllister RP, et al. Development of a cerebrospinal fluid lateral reservoir model in rhesus monkeys (*Macaca mulatta*). Comp Med. 2015;65(1):77-82. PubMed
3. Guide for care and use of laboratory animals. 8th ed. Washington, DC: The National Academies Press 2011. Online
4. Busch CM, Desai AV, Moorthy GS, Fox E, Balis FM. A validated HPLC-MS/MS method for estimating the concentration of the ganglioside, G_{D2}, in human plasma or serum. J Chromatogr B Analyt Technol Biomed Life Sci. 2018;1102-1103:60-65. CrossRef PubMed
5. Hobbs TR, Blue SW, Park BS, Greisel JJ, Conn PM, Pau FK. Measurement of blood volume in adult rhesus macaques (*Macaca mulatta*). J Am Assoc Lab Anim Sci. 2015;54(6):687-693. PubMed
6. Ladisch S, Wu ZL, Feig S, et al. Shedding of GD2 ganglioside by human neuroblastoma. Int J Cancer. 1987;39(1):73-76. CrossRef PubMed
7. Baratz E, McCully C, Shih J, Warren K. Comparison of pharmacokinetic parameters between non-human primates and human patients. Neuro-oncol. 2018;20(suppl 2):i157. CrossRef
8. Valentino LA, Ladisch S. Localization of shed human tumor gangliosides: association with serum lipoproteins. Cancer Res. 1992;52(4):810-814. PubMed

Journal of Circulating Biomakers

ABOUTSCIENCE